

https://dspace.org/

Enigmatic HighTenor Rh Ru Ir and OsRich Base Metal Sulfide Mineralization Within the Northern Limb of the Bushveld Complex A Product of Fractionation of a Sulfide Liquid

K.R Canham; D.A Holwell; L Du Preeze; Paul Nex; Allan Wilson ...

https://hdl.handle.net/10539/47153
WOS

Downloaded from a DSpace repository. https://dspace.org/

©2025 Society of Economic Geologists, Inc.
Economic Geology, v. 120, no. 4, pp. 997–1023

Enigmatic High-Tenor Rh-, Ru-, Ir-, and Os-Rich Base Metal Sulfide Mineralization Within the Northern Limb of the Bushveld Complex: A Product of Fractionation of a Sulfide Liquid?

Kate R. Canham,[1,†] David A. Holwell,[1] Lara Du Preez,[2] Paul AM. Nex,[3] Allan H. Wilson,[3] Katie McFall,[4] Erin S. Thompson,[1] Hannah SR. Hughes,[5] and Andy Lloyd[2]

[1] *Centre for Sustainable Resource Extraction, University of Leicester, University Road, Leicester, United Kingdom*

[2] *Anglo American South Africa, 144 Oxford Road, Rosebank, Johannesburg, South Africa*

[3] *School of Geosciences, University of the Witwatersrand, Johannesburg, South Africa*

[4] *Department of Earth Sciences, University College London, 5 Gower Place, London, United Kingdom*

[5] *Camborne School of Mines, Department of Earth and Environmental Sciences, University of Exeter, Penryn Campus, Penryn, Cornwall, United Kingdom*

Abstract

The Base Metal zone at Sandsloot in the Northern limb of the Bushveld Complex, South Africa, is a highly unusual and high-grade Os-Ir-Ru-Rh, Fe-Ni sulfide-rich horizon hosted within the deep Platreef, below the main platinum group element (PGE) horizon. The Base Metal zone ranges from 5 to 100 meters in thickness and is located up to 150 meters beneath the PGE reef. Base metal sulfide mineralization occurs as disseminated/blebby to semimassive/massive sulfides, with a typical assemblage of ~60/25/15 pyrrhotite/pentlandite/chalcopyrite modal %. The Base Metal zone is characterized by high (Os + Ir + Ru + Rh)/(Pt + Pd) ratios that reflect monosulfide solid solution, primitive mantle-normalized PGE profiles. The PGM assemblage is dominated by laurite (RuS_2) (62% by area) and iridium-group platinum group element (IPGE) + Pt arsenosulfides (21% by area). The PGE tenors of the sulfides vary between different textural styles, either reflecting R-factor variations or dilution of tenors by addition of crustal S. Disseminated/blebby sulfides have the highest tenors (up to 153 ppm Pd, 249 ppm Rh, 818 ppm Ru), whereas semimassive/massive sulfides have lower tenors (up to 2.8 ppm Pd, 1.8 ppm Pt, 11 ppm Rh, 17 ppm Ru, 2.2 ppm Os, 3.5 ppm Ir).

The PGE geochemistry, IPGE-dominant platinum group metal (PGM) assemblage, abundance of Fe sulfides, and high Ni/Cu ratios are consistent with the Base Metal zone representing the monsulfide solid solution portion of a sulfide liquid formed by fractional crystallization. Furthermore, the Cu + Pt + Pd + Au-poor nature of the Base Metal zone suggests that these metals were removed from the Base Metal zone, and some Cu-rich veins and sections are present around the margins of Ni-Fe sulfide to support this. Increasing Pd/Ir and decreasing Rh/Cu ratios downhole indicate the sulfide liquid fractionated downward. Therefore, a residual Cu-rich liquid, with associated Pt + Pd + Au, likely separated from monosulfide solid solution and was mobilized downward and away from the Base Metal zone. Significantly, the mobilization of a Cu-rich liquid leaves the possibility that an undiscovered Cu + Pt + Pd + Au orebody may exist at depth.

Introduction

The Northern limb of the Bushveld Complex is best known for the Critical zone-hosted Platreef deposit, which is one of the largest platinum group element (PGE) deposits in the world (Mudd et al., 2018). Within the Platreef, and PGE deposits more widely, palladium-group platinum group elements (PPGEs; Pt, Pd, and Rh) typically display greater enrichment than iridium-group platinum group elements (IPGEs; Ru, Os, and Ir). There are only a few rare occurrences where IPGEs + Rh are dominant over Pt + Pd in sulfide-dominant ores. Examples include contact-style pyrrhotite-rich ores at the Creighton PGE deposit, Sudbury (Dare et al., 2010a), pyrrhotite-rich ores at Skalisty mine, Norilsk-Talnakh (Tolstykh et al., 2022), and massive sulfides within the Eagle Ni-Cu-(PGE) deposit, Upper Michigan (Ding et al., 2012). These IPGE-rich ores all share a common theme—they are Fe sulfide-rich, massive to semimassive sulfides.

[†]Corresponding author: email, kkatecanham@googlemail.com

Discontinuous massive sulfide mineralization in the shallow Platreef is known to occur at several locations, such as at the base of the units at Tweefontein Hill (Nex, 2005) and Turfspruit (Sharman-Harris et al., 2005). Massive sulfides also occur within the footwall to the shallow Platreef at Overysel (Holwell and McDonald, 2006). More recently, drilling by Anglo American has identified disseminated to massive sulfide mineralization within the downdip extension of the Platreef (hereafter referred to as the deep Platreef) at Sandsloot, Mogalakwena mine complex. This sulfide mineralization is located 10s to 100s of meters beneath the PGE reef, the shallow equivalent of which is the mined horizon.

The sulfide-associated ores in the deep Platreef at Sandsloot are IPGE-Rh–dominant over Pt-Pd and thus represent a new style of mineralization in the context of the Platreef. We describe this IPGE-Rh mineralization in the lower portions of the deep Platreef at Sandsloot for the first time, presenting textural mineralogy, geochemistry, and sulfide and platinum-group mineral (PGM) analyses. We compare the style and composition of this massive sulfide mineralization at Sand-

ISSN 0361-0128; doi:10.5382/econgeo.5159; 27 p.
Digital appendices are available in the online Supplements section.

Submitted: November 22, 2024/Accepted: April 21, 2025

Downloaded from http://pubs.geoscienceworld.org/segweb/economicgeology/article-pdf/120/4/997/7306637/5159_canham+et+al.pdf
by University of the Witwatersrand user

sloot to other occurrences within the Platreef to demonstrate that the overall PGE contents are likely to be the product of variably fractionated and highly enriched sulfide liquid behavior during emplacement.

Background

The Northern limb of the Bushveld Complex

The 2.06 Ga (Zeh et al., 2015) Bushveld Complex, South Africa, hosts some of the world's largest magmatic sulfide deposits. It is divided into five geographically distinct limbs: the Western and Eastern limbs host the UG-2 and Merensky Reef deposits, while the Northern limb hosts the Platreef deposit (Cawthorn, 1999). The complex comprises the ultramafic-mafic Rustenburg Layered Suite, which intrudes into Paleoproterozoic sediments of the Transvaal Supergroup and Archean basement rocks. The Rustenburg Layered Suite is divided into five stratigraphic units: Marginal zone norites; Lower zone harzburgites and pyroxenites; Critical zone chromitites, pyroxenites, and norites; Main zone gabbronorites; and Upper zone anorthosites, gabbros, and magnetites (Hall, 1932; Cawthorn, 1999).

The Northern limb is a N-S–striking, westward-dipping sinuous outcrop extending over 120 km in length and 5 to 15 km in width. It is separated from the rest of the Bushveld Complex by the Thabazimbi-Murchison lineament (van der Merwe, 1976). The geology of the Northern limb has been described extensively in numerous publications (e.g., van der Merwe, 1976; Maier et al., 2008; McDonald and Holwell, 2011; Kinnaird and McDonald, 2018). It has mineralogical, stratigraphic, and geochemical differences from the other limbs. As such, there is much debate as to whether it can be directly correlated with the rest of the Bushveld Complex south of the Thabazimi-Murchison lineament (e.g., McDonald et al., 2005; van der Merwe, 2008; McDonald and Holwell, 2011; Yudovskaya et al., 2017; Maier et al., 2021). The limb hosts significant PGE + Ni + Cu mineralization throughout its stratigraphy; however, the most extensively studied and economically mined is the Platreef deposit. The Platreef is overlain by the Main zone and underlain by differing Paleoproterozoic sediments and Archaean gneiss/granite country rocks, or, in some locations, by the Lower zone (Fig. 1). The footwall rocks to the Platreef become successively older moving northward along strike. From south to north, the footwall rocks include the Timeball Hill-Magaliesberg Formation quartzites and shales, Duitschland Formation interbedded limestones and tuffs, Penge Formation banded ironstones, Malmani Subgroup dolomites and limestones, and Archean granites and gneisses (van der Merwe, 1976; Fig. 1).

The Platreef hosts a diverse range of Ni-Cu-PGE mineralization styles, including reef-style, disseminated, and massive contact-style sulfides. The high variability in mineralization styles along the Platreef's strike is partly attributed to differing metamorphic, metasomatic, and hydrothermal processes resulting from interaction with the highly heterogeneous footwall rocks (e.g., Harris and Chaumba, 2001; Armitage et al., 2002; Kinnaird et al., 2005; Holwell and McDonald, 2006, 2007; McDonald et al., 2009; van der Merwe et al., 2012; Yudovskaya et al., 2017). Net-textured and massive sulfides occur in the lower portions of the Platreef in several localities. At Tweefontein Hill (Fig. 1A), the development of massive sulfide mineralization, with an average thickness of 1.7 m, is thought to be related to the structure of the underlying footwall where sulfides accumulated in footwall depressions (Nex, 2005). In the Platreef at Turfspruit, minor massive and net-textured sulfides also occur toward the metasedimentary footwall (Hutchinson and Kinnaird, 2005; Kinnaird et al., 2005). In the Flatreef, the downdip extension of the Platreef at Turfspruit (Fig. 1), 1- to 3-m-thick massive sulfide pods occur beneath the PGE reef within a package of contaminated parapyroxenites, paraperidotites, and calc-silicates (Yudovskaya et al., 2017). Net-textured and massive sulfides also occur within the gneiss footwall at Overysel (Fig. 1); these appear to have formed when fractionating sulfide liquid percolated downward from the Platreef and accumulated in a partially molten footwall (Holwell and McDonald, 2007).

Recent research in and around the Mogalakwena Mine Complex in the Northern limb

This work is part of a series of papers (see Canham et al., 2025; Thompson et al., 2025a, b; Thompson et al., 2025a-c) presenting new data for the Northern limb associated with extensive recent drilling conducted by Anglo American. These studies cover aspects of the magmatic emplacement and associated mineralization in the Lower zone and both shallow and deep Platreef at Tweefontein, Sandsloot, Zwartfontein, and Overysel within the Mogalakwena Mine Complex and adjacent exploration properties (Fig. 1A). A brief overview of these works is provided below for context.

Canham et al. (2025) describe the Zwartfontein Lower zone chromitite-associated PGE + Ni + Cu mineralization, located north of Sandsloot (Fig. 1A). They propose a model in which localized carbonate and volatile assimilation triggered in situ chromite nucleation and sulfide saturation. Thompson et al. (2025a) use the Platreef as a case study to demonstrate the application of Niggli Numbers, comparing contamination signatures with Ni-Cu-PGE–grade variations along strike of the Platreef (Tweefontein to Overysel; Fig. 1A). They suggest the deep Platreef at Sandsloot, and specifically the Base Metal zone, which is the focus of this study, has some characteristics of a skarn-like system where carbonate assimilation may have acted to upgrade or generate PGE-Ni-Cu mineralization. Thompson et al. (2025b) focus on the magmatic history of the Platreef at Tweefontein, located south of Sandsloot (Fig. 1A), proposing a complex multisill emplacement model.

Most relevant to this study on the Base Metal zone at Sandsloot is Thompson et al. (2025c), who give the first description of the stratigraphy of the deep Platreef at Sandsloot, using whole-rock geochemistry, silicate petrology, and silicate mineral chemistry to define several discreet units within the deep Platreef. The following stratigraphic framework for the deep Platreef at Sandsloot, defined by Thompson et al. (2025c), is followed throughout this paper: (1) the Fly, (2) the PGE reef, which is the downdip extension of the mined horizon, (3) the Subreef and Subreef pyroxenite, (4) the Base Metal zone, and (5) the Sub-Base Metal zone (Fig. 1B). The uppermost unit of the deep Platreef, the Fly, is characterized by homogeneous feldspathic pyroxenites with limited carbonate contamination. Underlying this is the PGE reef, which is the most Pt + Pd-enriched portion of the deep Platreef and

Downloaded from http://pubs.geoscienceworld.org/segweb/economicgeology/article-pdf/120/4/997/7306637/5159_canham+et+al.pdf
by University of the Witwatersrand user

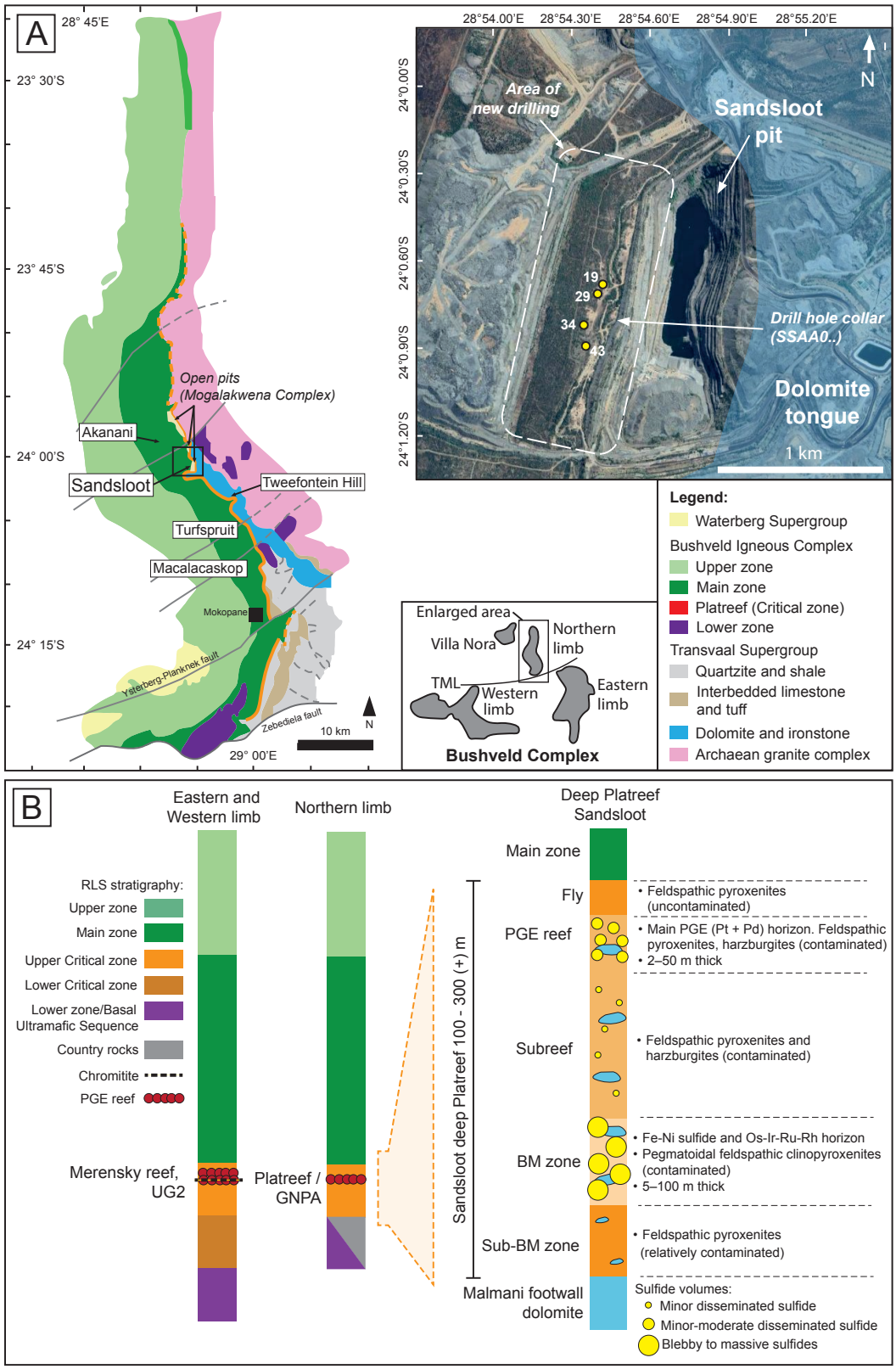

Fig. 1. (A) Geologic map of the Northern limb with Sandsloot and other localities referenced annotated (adapted from van der Merwe, 1976, and further modified using adaptions from Ashwal et al., 2005; Van der Merwe et al., 2012; Kinnaird and McDonald, 2018). Satellite image of the area of drilling intersecting the downdip Platreef is also shown. (B) Simplified stratigraphic log of the Rustenburg Layered Suite (RLS) in the Eastern and Western limb correlated to the Northern limb (after White, 1994) and the deep Platreef at Sandsloot (after Thompson et al., 2025c). BM zone = Base Metal zone, PGE = platinum group element, TML = Thabazimbi-Murchison lineament

Downloaded from http://pubs.geoscienceworld.org/segweb/economicgeology/article-pdf/120/4/997/7306637/5159_canham+et+al.pdf
by University of the Witwatersrand user

is characterized by altered feldspathic pyroxenites that are highly carbonate contaminated. Beneath the PGE reef is the Subreef, which is lithologically similar to the PGE reef and highly carbonate contaminated but lacks significant PGE mineralization. The Base Metal zone is characterized by pegmatoidal feldspathic clinopyroxenites. It is sulfide + PGE rich and also highly carbonate contaminated. The transition from the Base Metal zone into the underlying Sub-Base Metal zone is marked by the return to feldspathic pyroxenites, with orthopyroxene as the dominant mineral (Thompson et al., 2025c).

In this contribution, we specifically examine the ore mineralogy of the Base Metal zone at Sandsloot and its newly recognized IPGE + Rh-rich nature, presenting details on the metal tenors and PGE and sulfide mineralogy for the first time.

Sampling and Analytical Methods

Drill cores SSAA019, SSAA043, SSAA034, and SSAA029 (SA19, SA43, SA34, SA29) (Fig. 1) were selected for sampling. These drill cores were selected as they intersect a range of sulfide textures and Cu + Ni + PGE grades. Twelve quarter core samples of 30 to 50 cm were sampled from the Base Metal zone, and three additional samples were taken from above and below the Base Metal zone in SA43 (Table 1). Thin sections were prepared from these samples at the University of Leicester, and the remaining material was crushed and milled using steely fly press and agate ball mills in preparation for bulk-rock geochemical analysis.

Geochemistry

Whole-rock metal grades are discussed as ratios and relative terms only throughout the manuscript due to commercial sensitivity. Bulk-rock major element oxide geochemistry of ~1-m intervals downhole and Cu, Ni, Pt, Pd, Co, and Au assays were provided by Anglo American. Rhodium assays were available when Pt + Pd values were over a certain threshold (>1 ppm). Major element analyses were undertaken on glass discs produced by borate fusion followed by X-ray fluorescence (XRF); the trace element analyses were conducted for Cu + Ni + Co through pressed-pellet XRF and for PGE + Au through Pb fire assay with ICP-OES finish at SGS Laboratories, South Africa. The additional 15 quarter core samples selected for this study were analyzed for trace elements by XRF on pressed powder pellets at the University of Leicester and by four-acid digestion with inductively coupled plasma-atomic emission spectroscopy (ICP-AES) (ALS method code: ME-ICP61) at ALS Geochemistry, Loughrea, Ireland. Reference materials (OREAS 141/137/924/195, MRGeo08, EMOG-17) were analyzed to monitor data quality. The percentage relative difference (RD%) of the relevant trace elements range from 1.6 to 7.8% and percentage relative standard deviation (RSD%) from 0 to 4.3%, classified as very good, following Piercey (2014). A subset of samples (n = 6) was analyzed for full 6PGE (Os, Ir, Ru, Rh, Pt, Pd) geochemistry by Ni sulfide fire assay with inductively coupled plasma-mass spectrometry (ICP-MS; ALS method code: PGM-MS25NS) by ALS Geochemistry, Johannesburg. Standards OREAS684/683 and AMIS0498 alongside blanks and repeats were also run. The %RD and %RSD range from 2.5 to 9.4 and 0 to 4.3%, respectively.

Intersections of net-textured sulfides from the shallow Platreef at Tweefontein Hill (Fig. 1A) were sampled from TN190D1 (App. Fig. A1). These were used for comparison of PGE + Ni + Cu patterns between the Base Metal zone and semimassive sulfides elsewhere in the Platreef. Samples were crushed and milled for bulk-rock analysis and analyzed for 6PGE + Au by Ni-S fire assay followed by ICP-MS at the School of Geosciences, University of KwaZulu-Natal (while

Table 1. Table Summarizing the Lithology and Sulfide Texture of Samples from this Study

Hole	Depth (m)	Zone	Lithology	Sulfide texture 1	Sulfide texture 2	Pt + Pd + Au grade	IPGE + Rh grade
SA19	705	BM Zone	BMS pegmatoidal feldspathic clinopyroxenite	Semimassive/massive	Net textured	Low	High
SA19	724	BM Zone	BMS feldspathic clinopyroxenite	Semimassive/massive	Semimassive	Low	NA
SA19	726A	BM Zone	BMS feldspathic clinopyroxenite	Semimassive/massive	Massive symplectic	Low	High
SA19	726B	BM Zone	BMS pegmatoidal feldspathic clinopyroxenite	Semimassive/massive	Semimassive symplectite	Low	High
SA19	727	BM Zone	BMS feldspathic pyroxenite	Semimassive/massive	Vein (fractionated)	Low	High
SA19	729A	BM Zone	BMS feldspathic clinopyroxenite	Semimassive/massive	Semimassive symplectite	Low	High
SA19	729B	BM Zone	BMS sulfide feldspathic pyroxenite	Semimassive/massive	Net textured	Low	High
SA19	749	BM Zone	Massive BMS	Semimassive/massive	Massive	Low	Low
SA19	750	BM Zone	BMS feldspathic clinopyroxenite	Semimassive/massive	Semimassive symplectite	Low	NA
SA29	761	BM Zone	Clinopyroxenite	Disseminated/blebby	Disseminated/blebby	Moderate	NA
SA34	769	BM Zone	Serpentinized feldspathic clinopyroxenite	Disseminated/blebby	Disseminated	Low	NA
SA34	772	BM Zone	Feldspathic clinopyroxenite	Disseminated/blebby	Blebby	Low	NA
SA34	780	BM Zone	Pegmatoidal feldspathic clinopyroxenite	Disseminated/blebby	Disseminated	Low	NA
SA43	764	Above BM Zone	Pyroxenite (altered)	Disseminated/blebby	Blebby	Low	NA
SA43	769	Above BM Zone	Pyroxenite	Disseminated/blebby	Disseminated	Low	NA
SA43	791	BM Zone	Pegmatoidal feldspathic clinopyroxenite	Disseminated/blebby	Blebby, minor vein	High	Very high
SA43	794	Sub-BM Zone	Pyroxenite (altered)	Vein	Vein (with calcite)	Moderate	NA

Notes: Sulfide texture 1 refers to the sulfide texture group the sample is assigned; sulfide texture 2 is a more detailed description of the sulfide texture; NA = not applicable

Abbreviations: BMS = base metal sulfide, BMZ = Base Metal zone, IPGE = iridium-group platinum group element

Downloaded from http://pubs.geoscienceworld.org/segweb/economicgeology/article-pdf/120/4/997/7306637/5159_canham+et+al.pdf
by University of the Witwatersrand user

lab was under supervision of A.W.). International reference materials SARM6 and SARM7 were analyzed alongside repeats. Copper and Ni were determined through pressed-pellet XRF (error ranges from 0.3–1.1%). Full details of the limits of detection, alongside accuracy and precision estimates for all whole-rock geochemical analyses, are available in Appendix Table A1.

Trace elements in sulfides

The concentrations of trace elements in sulfide were established by laser ablation-inductively coupled plasma-mass spectrometry (LA-ICP-MS) analysis at the University of Leicester, using a ThermoScientific ICAP-Qc quadrupole ICP mass spectrometer, equipped with a New Wave Research-ESI 213-nm laser unit, following methods outlined in Barnes et al. (2020), Tolstykh et al. (2022), and Blanks et al. (2022). Track ablations were performed at a spot size of 50 µm, laser frequency of 5 µm, pulse rate of 10 Hz, and fluence of 3.5 to 4 J/cm^2. Total acquisition lasted 90 to 120 s, including 30 s of gas background prior to ablation. The following isotopes were measured: ^{28}Si, ^{29}Si, ^{33}S, ^{47}Ti, ^{49}Ti, ^{53}Cr, ^{57}Fe, ^{59}Co, ^{60}Ni, ^{61}Ni, ^{63}Cu, ^{66}Zn, ^{68}Zn, ^{75}As, ^{77}Se, ^{82}Se, ^{101}Ru, ^{103}Rh, ^{105}Pd, ^{107}Ag, ^{108}Pd, ^{121}Sb, ^{125}Sb, ^{185}Re, ^{189}Os, ^{193}Ir, ^{195}Pt, ^{197}Au, ^{208}Pb, and ^{209}Bi. Data reduction was carried out using iolite v.4 software. To mitigate the effect of ablating any microinclusions, scanning electron microscopy (SEM) surveys were carried out prior to LA-ICP-MS analyses to identify any visible microinclusions. Time-resolved analysis (TRA) spectra were also monitored, and any PGM microinclusions were manually excluded. Additionally, Cr, Ti, and Si were monitored to ensure no silicate or oxides were included in the analyses.

Calibration was carried out using UQAC-FeS1 on ^{33}S (Holwell et al., 2015; McFall et al., 2019). This was measured between changing samples and every 20 to 30 minutes during analysis to account for any instrument drift. To check for interferences, multiple isotopes for elements were collected. It is known that ^{105}Pd is interfered by ^{65}Cu^{40}Ar; therefore, we used ^{108}Pd. ^{108}Pd is interfered by ^{68}Zn^{40}Ar and ^{108}Cd, so ^{68}Zn and ^{108}Cd were monitored. For pyrrhotite and pentlandite, Zn and Cd concentrations were both low (below 10 ppm), so no correction was needed. However, Zn was very high in chalcopyrite (up to 1,007 ppm), resulting in significant interferences on ^{108}Pd; thus, no Pd concentrations are reported for chalcopyrite. ^{103}Rh is interfered by ^{63}Cu^{43}Ar, so no ^{103}Rh values are reported for chalcopyrite. To monitor results, MASS-1 was measured when changing samples and at the beginning and end of the day. The %RSD and %RD of PGEs range from 6.2 to 9.8 and 5.6 – 11.0%, respectively (full accuracy and precision are given in App. Table A2 and detection limits in App. Table A4).

PGM studies

Seven thin sections were analyzed for PGMs by energy-dispersive X-ray spectroscopy (EDS) analysis using a ZEISS Sigma field emission scanning electron microscope equipped with two Bruker 6l30 EDX detectors at the University of Leicester. The thin sections were chosen based on their assay grade and sulfide textures to ensure a spread of samples throughout the Base Metal zone. Samples were mapped using the automated mapping software ZEISS Mineralogic. The sample run conditions were set to a magnification of 250 to 500×, step size of 1 µm^2, dwell time of 0.25 s, accelerating voltage of 20 kV, and aperture of 120 µm. As PGMs and precious metal minerals (PMMs) have high specific gravity, they appear bright under backscattered electron (BSE) imaging relative to sulfides and silicates; therefore, a bright phase threshold was established so any phases (PGM and PMM) over the assigned brightness threshold would be identified and mapped. Additionally, the area to be mapped was dilated by 3× to incorporate the surrounding host mineral and gain information on each PGM's association. During analysis, the area (µm^2), Feret max diameter (µm), and semiquantitative composition (wt %) of each PGM was recorded. The measured stoichiometric values were then used to assign each PGM a name from a custom-designed PGM library. After the automated analysis, PGMs were individually revisited manually to gain broader association data and collect high-quality photomicrographs.

Mineral maps

The same seven thin sections analyzed for PGMs were also analyzed by automated, quantitative SEM mapping to produce mineral maps using ZEISS Mineralogic software (Holwell et al., 2017). The remaining thin sections were assessed optically to ensure findings are consistent across the samples. The analysis was performed at operating conditions of 20 kV, a working distance of 8.5 mm, and an aperture of 120 µm. A dwell time of 0.05 s and a step size of 25 to 40 µm^2, varying depending upon grain size, was utilized. Counts for EDS detection were consistently above 3,000.

Stratigraphy

The Base Metal zone is located in the deep Platreef at Sandsloot. We use the term deep Platreef throughout this study to refer to the rocks that occur between the Main zone and the metasedimentary footwall or Lower zone (Fig. 1B). In the deep Platreef at Sandsloot, PGE + Ni + Cu mineralization is contained within two key horizons: (1) the PGE reef, the shallow equivalent of which is the mined horizon and (2) the Base Metal zone, which is the focus of this study. Footwall rocks have, as of yet, not been intersected below the deep Platreef at Sandsloot.

The Base Metal zone lies ~50 to ~150 m beneath the PGE reef. The relative proportion of Ni, Cu, and Pt + Pd within the Base Metal zone compared to the overlying PGE reef is outlined in Figure 2A for drill holes SA43 and SA19, which are considered representative of the Base Metal zone (logs for additional holes sampled are provided in App. Fig. A1). The Base Metal zone is variably developed, ranging in thickness from 5 m (e.g., in SA43) to ~100 m (e.g., in SA19). The intensity of Ni-Cu-PGE sulfide mineralization within the Base Metal zone is also highly variable; sulfides occur as disseminated/blebby sulfides only in some holes (e.g., SA43, SA34; Fig. 2B), while other holes intersect semimassive/massive sulfides (SA19; Fig. 2A). Above and below the Base Metal zone is a series of pyroxenites and feldspathic pyroxenites that can be highly altered.

Petrology

To conform to previous studies of the Northern limb (e.g., Harris and Chaumba, 2001; Armitage et al., 2002; McDonald et al., 2005; Holwell et al., 2006), we follow general Bush-

Downloaded from http://pubs.geoscienceworld.org/segweb/economicgeology/article-pdf/120/4/997/7306637/5159_canham+et+al.pdf
by University of the Witwatersrand user

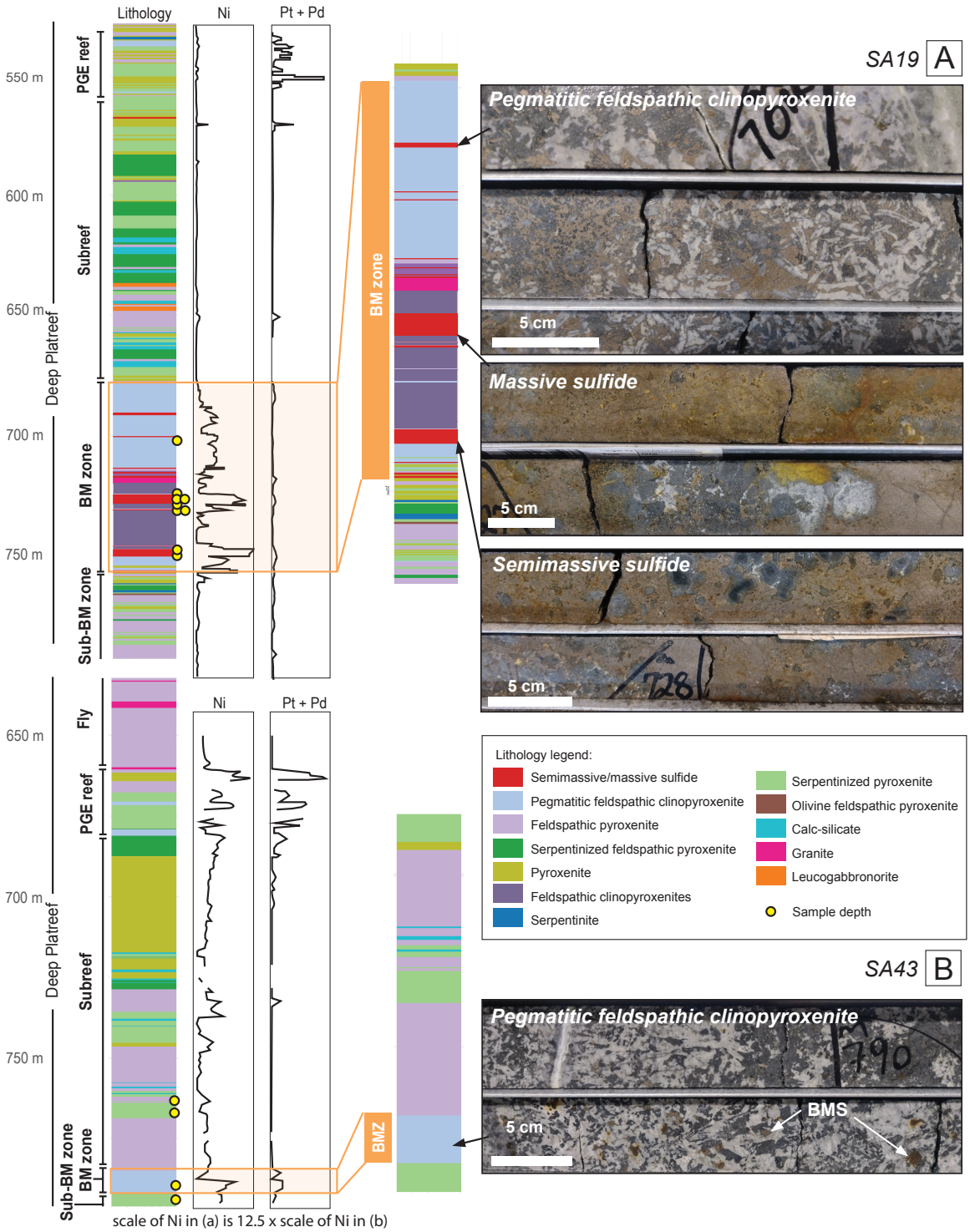

Fig. 2. Downhole stratigraphic and lithological logs alongside downhole metal geochemistry (Ni and Pt + Pd) of (A) SA19 and (B) SA43 through the deep Platreef at Sandsloot; the Base Metal zone (BM zone; BMZ) is highlighted. Scale for Ni and Cu are not the same in (A) and (B). Photographs of core in the Base Metal zone are also shown. Data for stratigraphic and assay logs was provided by Anglo American. BMS = base metal sulfide.

veld nomenclature. Therefore, we use the terms feldspathic clinopyroxenites and pegmatoidal feldspathic clinopyroxenites, even though these rocks would instead be classified as gabbronorites and gabbros under the International Union of Geological Sciences (IUGS) classification. Here we describe the petrology of the rocks that host the disseminated to blebby and semimassive to massive sulfides of the Base Metal zone at Sandsloot. Further details on the geochemistry and nature of this unit within the broader stratigraphy at Sandsloot can be found in Thompson et al. (2025c).

Downloaded from http://pubs.geoscienceworld.org/segweb/economicgeology/article-pdf/120/4/997/7306637/5159_canham+et+al.pdf
by University of the Witwatersrand user

The Base Metal zone at Sandsloot comprises pegmatoidal feldspathic clinopyroxenites (with a notable absence of orthopyroxene, which is generally the dominant pyroxene in Platreef rocks), pegmatoidal clinopyroxenites, feldspathic clinopyroxenites, and massive sulfides. Pegmatoidal feldspathic clinopyroxenites (Fig. 2) comprise coarse-grained plagioclase (40–60 modal %) and clinopyroxene (40–60 modal %; Fig. 3A). Plagioclase tends to form coarse-grained laths (up to 2 cm) and is extensively altered to prehnite (Fig. 3A, B); clinopyroxene may also be coarse grained (up to 0.5 cm) or medium to fine grained (0.5–2 mm) and subhedral (Fig. 3B). Feldspathic clinopyroxenites comprise clinopyroxene (50–85 modal %), plagioclase (15–50 modal %), and minor orthopyroxene (<10 modal %). Fine-grained (0.1–0.5 mm) clinopyroxene and plagioclase can form an amoeboid granoblastic texture (Fig. 3B) or irregular coarser grains. Pegmatoidal clinopyroxenites comprise clinopyroxene (85–90 modal %) and plagioclase (<15 modal %). Clinopyroxene is typically coarse grained (up to 1.5 cm) with fine-grained intergrowths of plagioclase (Fig. 3C). Sections of finer grained subhedral clinopyroxene (0.5–2 mm) with interstitial plagioclase are also present. Massive sulfides are described in the subsequent section. They occur where sulfide constitutes >80 modal % of the rock, with lesser clinopyroxene, plagioclase, and Fe oxides.

Accessory minerals seen in all lithologies include magnetite, ilmenite, and apatite. Disseminated ilmenite and magnetite

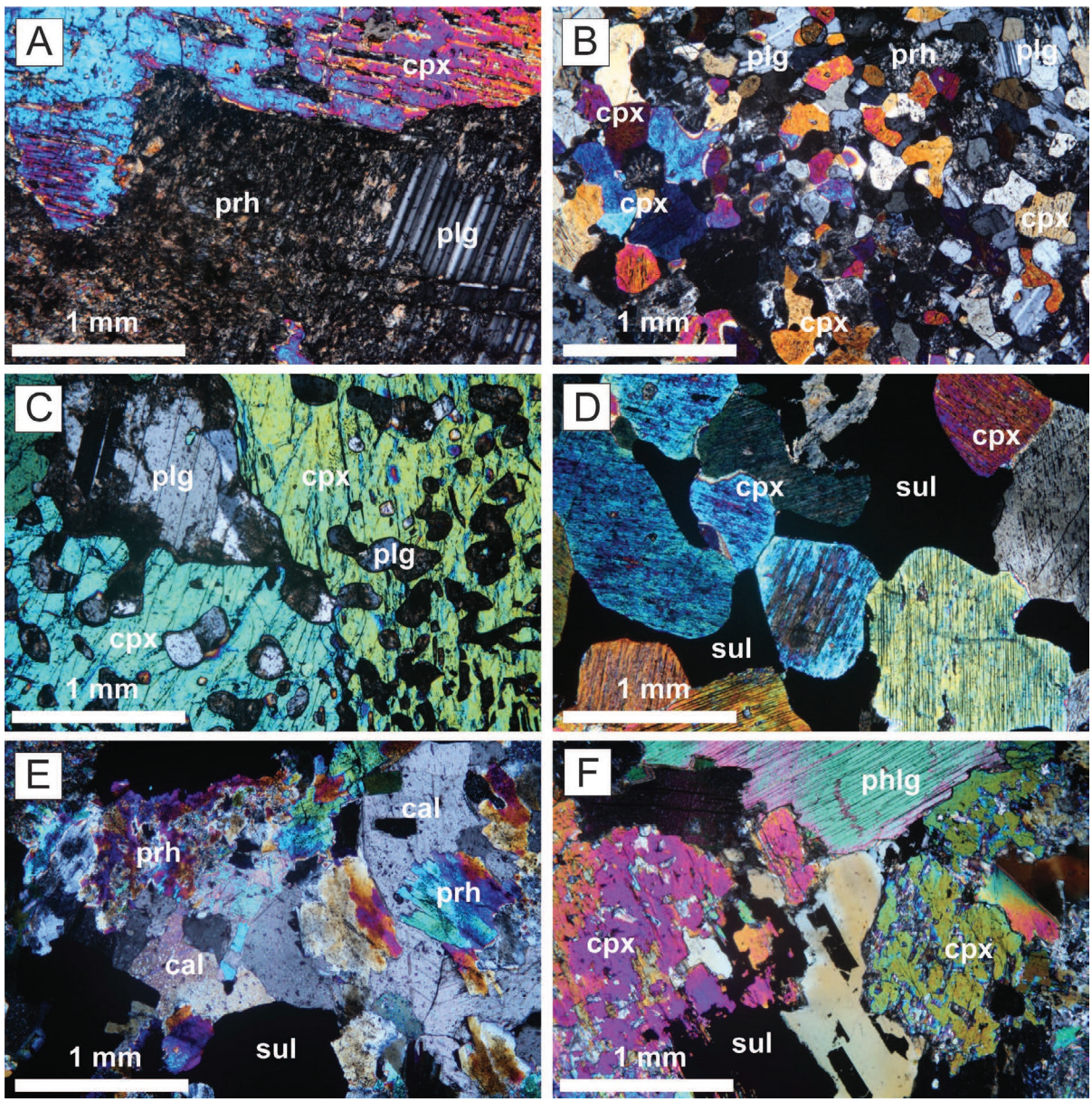

Fig. 3. Photomicrographs of typical textures in the Base Metal zone in cross-polarized transmitted light: (A) pegmatoidal clinopyroxene and plagioclase; plagioclase is near totally replaced by prehnite; (B) fine-grained amoeboid granoblastic plagioclase and clinopyroxene; (C) coarse-grained clinopyroxene with plagioclase intergrowths; (D) medium-grained rounded clinopyroxene, with sulfide; (E) calcite and prehnite alteration; (F) phlogopite, sulfide, and hornblende within clinopyroxenite. Abbreviations: cal = calcite, cpx = clinopyroxene, phlg = phlogopite, plg = plagioclase, prh = prehnite, sul = sulfide.

Downloaded from http://pubs.geoscienceworld.org/segweb/economicgeology/article-pdf/120/4/997/7306637/5159_canham+et+al.pdf
by University of the Witwatersrand user

(<1 modal %) are common in association with disseminated/blebby sulfides, and where semimassive to massive sulfides are present, magnetite + ilmenite is often more abundant (0–15 modal %). Calcite is also commonly observed, and often this is associated with sulfide (Fig. 3E).

The rocks within the Base Metal zone have experienced variable degrees of alteration. In addition to the prehnite alteration of plagioclase, clinopyroxene can be partially to completely altered to talc. Where alteration is more extensive, phlogopite and hornblende occur as accessory phases, along with extensive chlorite and serpentine (Fig. 3F).

Sulfide Mineralogy

Sulfide mineralization in the Base Metal zone at Sandsloot is present as disseminated to blebby, vein, semimassive (including net-textured), and massive sulfides. On the whole, sulfides are predominantly pyrrhotite, with lesser pentlandite and chalcopyrite, in an average modal % of ~60/25/15 pyrrhotite/pentlandite/chalcopyrite. A summary of the sulfide textures for each sample is provided in Table. 1.

Semimassive to massive sulfides

Pyrrhotite is the dominant sulfide within massive/semimassive sulfides, followed by pentlandite, with lesser chalcopyrite. Pentlandite is present as loops around pyrrhotite (Fig. 4A, C), as exsolution flames within pyrrhotite, and along fractures within pyrrhotite (Fig. 4B). Chalcopyrite is typically separated and restricted to the boundaries of the semimassive/massive sulfides (Fig. 4C) and is also present in Cu-rich sulfide veins at the peripheries of Fe-Ni sulfide patches (Fig. 4D).

In massive/semimassive sulfides, a common texture within pegmatoidal clinopyroxenites is coarse-grained sulfide-clinopyroxene symplectites (Fig. 4C, E). Surrounding the sulfide symplectite are worm-like intergrowths of plagioclase, sulfides ± magnetite, ilmenite, and clinopyroxene (Fig. 4E). In pegmatoidal feldspathic clinopyroxenites, sulfides are typically net textured, and networks of sulfides are distributed between coarse plagioclase laths (Fig. 4F). Net-textured sulfides are grouped under semimassive/massive sulfides.

Magnetite is present along fractures within sulfides and also occurs as coarse-grained, subrounded inclusions (up to 3 mm) with ilmenite within sulfide (Fig. 4G). Calcite inclusions are common in massive sulfides and are often rimmed by chalcopyrite (Fig. 4B).

Disseminated to blebby sulfides

Blebby sulfides (<10 modal % sulfide) are up to 1 cm and predominantly pyrrhotite with pentlandite rims (Fig. 5A). Minor chalcopyrite may also be present within the rims; however, chalcopyrite tends to form separate, smaller sulfide blebs (<2 mm) that are chalcopyrite-dominant, with pyrrhotite and pentlandite around their boundaries. Calcite blebs are commonly found within the chalcopyrite-dominant sulfides (Fig. 5A, C). As with the massive sulfides, magnetite often occurs along sulfide fractures.

Vein sulfides

Coarse-grained sulfide veins (Fig. 5D, E), up to 1 cm thick, are typically associated with highly altered lithologies, where abundant chlorite and accessory phlogopite and hornblende is present. Fine-grained sulfide veins (<0.1 mm) are often chalcopyrite dominant (Fig. 5F, G). Sulfide veins typically also contain calcite. Sulfide veins with pentlandite and pyrrhotite separated from chalcopyrite are also noted in intersections of massive sulfide (Fig. 4D).

Whole-Rock Geochemistry

Downhole geochemistry

Selected whole-rock geochemistry and ratios of samples from this study are provided in Table 2. Figure 6 shows the downhole variation of base and precious metals (Ni, Cu, Pt, Pd, Co, Au) as well as CaO, MgO, Al_2O_3, Fe_2O_3, and TiO_2 through two drill holes that intersect the Base Metal zone—the first intersecting semimassive/massive sulfide mineralization (Fig. 6A) and the second intersecting disseminated to blebby sulfides (Fig. 6B). Downhole geochemical logs for the additional holes sampled are available in Appendix Figure A1.

In the drill hole containing intersections of semimassive/massive sulfides (Fig. 6A), two significant intersections of semimassive to massive sulfides occur, from 724 to 731 and 745 to 758 m. Above and between these two zones, disseminated/blebby sulfides are present; as such, Ni and Cu are still elevated, but to a lesser extent. High abundances of Fe_2O_3 and S correlate with zones of massive sulfide, with S ranging from 7 wt % in semimassive sulfides up to 34 wt % in massive sulfides (Table 2). Increases in Al_2O_3 (up to 15 wt %) relate to increase in the modal proportion of plagioclase and prehnite after plagioclase. High CaO contents (>10 wt %) reflect the abundance of clinopyroxene, and low MgO contents (<10 wt %) are due to the lack of olivine and orthopyroxene. Below the Base Metal zone, the Sub-Base Metal zone is marked by an increase in MgO (15–40 wt % MgO) as serpentinized pyroxenites and harzburgites become more dominant. Bulk TiO_2 is very low (<0.02 wt %) in the first massive sulfide intersection but increases in the second massive sulfide intersection to 0.2 to 0.7 wt %. The Cr_2O_3 contents are consistently low (<0.02 wt %) within the Base Metal zone. Granitic intersections are present in places and correlate with CaO/Al_2O_3 decreases (<0.5) and SiO_2 increases.

In drill holes containing blebby and disseminated sulfides (as exemplified by the drill hole intersection in Fig. 6B) the Base Metal zone can vary in thickness, ranging from 5 m (e.g., SA43; Fig. 6B) to 110 m (e.g., SA56). Sulfur concentrations range from 0.8 to 2.7 wt % (Table 2). As in the semimassive/massive sulfides, MgO decreases from the unit above into the Base Metal zone (<10 wt %), while Al_2O_3 (>10 wt %) and CaO (>11 wt %) increase, reflecting an increase in the proportion of clinopyroxene and plagioclase in the Base Metal zone. Unlike the semimassive/massive sulfides, Fe_2O_3 decreases from the unit above, due to the increase of plagioclase, reduction in pyroxene and olivine, and a lesser amount of sulfide (Fig. 6B).

Chalcophile element geochemistry

Copper and Ni grades are controlled by the amount of sulfide. Nickel and Cu reach high and moderate grades, respectively, in intersections of semimassive/massive sulfides (Fig. 6A) and lower grades in blebby/disseminated sulfides (Fig. 6B). Within intersections of blebby/disseminated sulfides (Fig. 6B) Pt +

Downloaded from http://pubs.geoscienceworld.org/segweb/economicgeology/article-pdf/120/4/997/7306637/5159_canham+et+al.pdf
by University of the Witwatersrand user

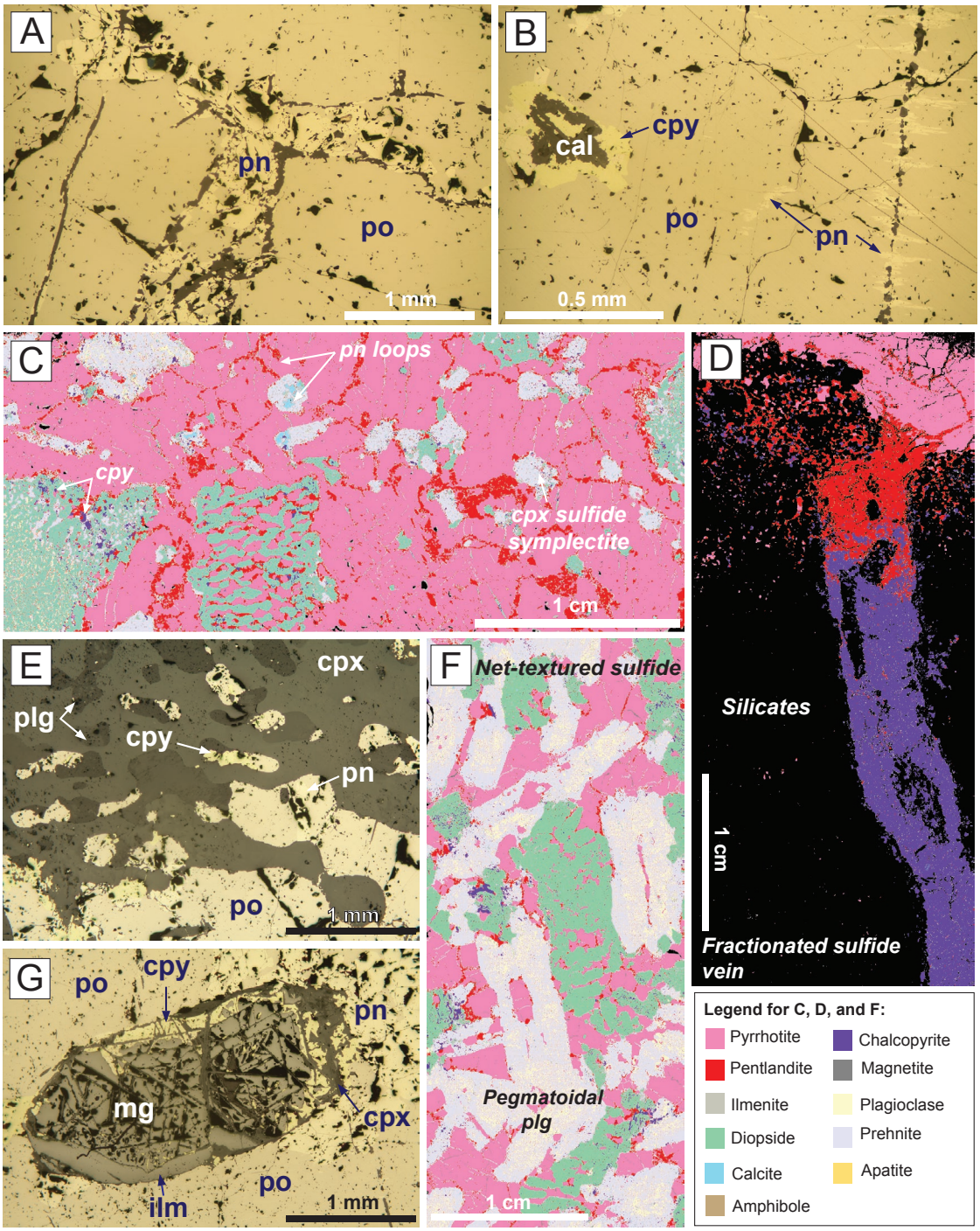

Fig. 4. (A, B, E, G) Photomicrographs and (C, D, F) mineral maps of typical textures in the semimassive to massive sulfides in the Base Metal zone: (A) pentlandite loops within pyrrhotite; (B) pentlandite exsolution within pyrrhotite and chalcopyrite around calcite; (C) symplectite sulfide-silicate texture with pentlandite loops and chalcopyrite separated and toward the boundary of the symplectite; (D) fractionated sulfide vein; (E) symplectite sulfide and silicates, including clinopyroxene and plagioclase variably altered to prehnite; (F) semimassive net-textured sulfide with coarse-grained plagioclase laths; and (G) coarse-grained magnetite and ilmenite with chalcopyrite around its boundary, hosted within massive sulfide. Abbreviations: cal = calcite, cpx = clinopyroxene, cpy = chalcopyrite, ilm = ilmenite, mg = magnetite, plg = plagioclase, pn = pentlandite, po = pyrrhotite.

Pd grades range from moderate to high, whereas IPGE and Rh abundances are very high, and Co is up to 261 ppm. In contrast, Pt and Pd are low within the semimassive/massive sulfides (Fig. 6A), whereas IPGE + Rh are higher, as is Co (up to 1,480 ppm). The (Os + Ir + Ru + Rh)/(Pt + Pd) ratio within the Base Metal zone ranges from 0.6 to 22.4 (avg 9.6).

Within the semimassive/massive sulfides Ni/Cu ratios average 5.4, ranging from 2 to 20 (Fig. 7A). Platinum and Pd

Downloaded from http://pubs.geoscienceworld.org/segweb/economicgeology/article-pdf/120/4/997/7306637/5159_canham+et+al.pdf
by University of the Witwatersrand user

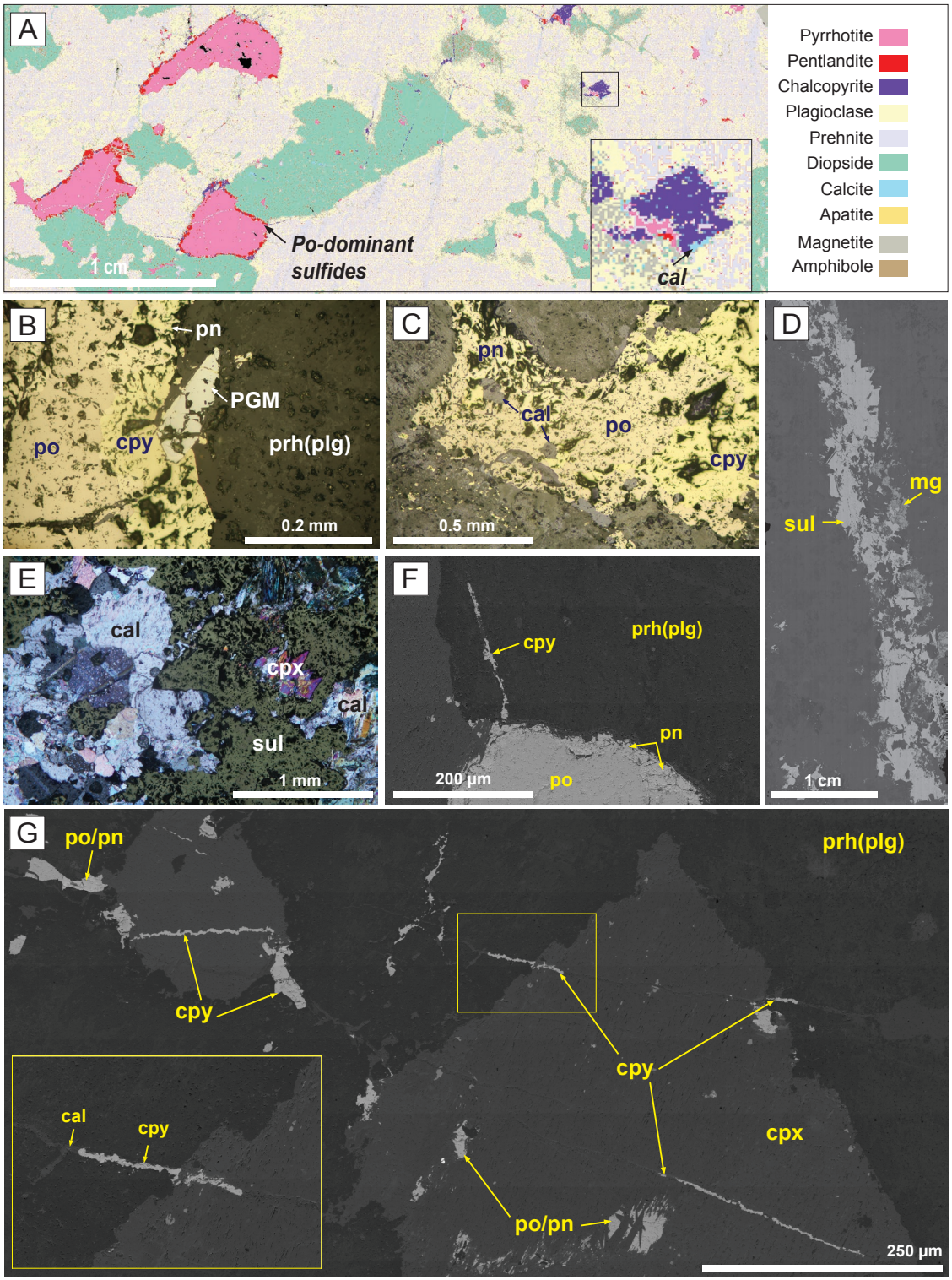

Fig. 5. Photomicrographs, backscattered electron (BSE) images and mineral maps of (A-C) disseminated/blebby and (D-G) vein sulfide textures in the Base Metal zone. (A) Mineral map of blebby sulfides, highlighting the pyrrhotite-rich nature of the sulfide ores. Also note the association of calcite with chalcopyrite-rich sulfide blebs. Photomicrographs of (B) pentlandite and chalcopyrite rims around pyrrhotite and (C) pyrrhotite, chalcopyrite, pentlandite sulfide bleb containing calcite inclusions. (D) BSE image of sulfide (pyrrhotite, pentlandite, and chalcopyrite) vein with magnetite. (E) Photomicrograph showing enlarged view of sulfide vein in (D), showing calcite hosted alongside sulfide in the vein; vein is wider than the view diameter. (F) BSE image of separation of chalcopyrite from pentlandite and pyrrhotite. (G) BSE image of chalcopyrite ± calcite veins crosscutting silicates. Pyrrhotite and pentlandite occur as blebs that are overprinted by secondary silicates. Abbreviations: cal = calcite, cpy = chalcopyrite, cpx = clinopyroxene, mg = magnetite, pn = pentlandite, po = pyrrhotite, prh(plg) = prehnite-altered plagioclase, sul = sulfide.

Downloaded from http://pubs.geoscienceworld.org/segweb/economicgeology/article-pdf/120/4/997/7306637/5159_canham+et+al.pdf
by University of the Witwatersrand user

Table 2. Ratios of Trace Elements and PGEs for the Base Metal Zone at Sandsloot

Hole	Depth (m)	Zone	Alt	Sulfide texture	IPGE/ PPGE	IPGE+ Rh/ Pt + Pd	Pt/ Pd	Ni/Cu	Au/Pd	Pd/ Ir	Rh/ Ir	Rh/Pd	(Rh/Cu) *10^7	S/Se	S (%)
SA19	705	BM Zone	maj	semimassive/massive	2.26	22.42	0.35	3.94	0.13	0.35	2.93	8.36	4.416	5,702	9.58
SA19	724	BM Zone	maj	semimassive/massive	NA	NA	0.21	10.50	0.14	NA	NA	3.08	15,448	8,830	22.87
SA19	726A/B	BM Zone	min	semimassive/massive	1.41	12.21	0.39	17.79	0.08	0.41	2.56	6.25	22,663	8,393	25.77
SA19	727	BM Zone	mod	semimassive/massive (vein)	1.29	10.84	0.41	21.62	0.12	0.43	2.50	5.88	28,902	7,691	25.61
SA19	729A/B	BM Zone	mod	semimassive/massive	1.48	8.01	0.67	8.66	0.06	0.73	3.20	4.41	15,573	7,394	6.95
SA19	749	BM Zone	mod	semimassive/massive	0.07	0.59	0.28	5.34	0.11	20.83	12.74	0.61	910	8,175	34.17
SA19	750	BM Zone	min	semimassive/massive	NA	NA	0.64	5.59	0.18	NA	NA	0.38	627	6,567	13.07
SA29	761	BM Zone	min	disseminated/blebby	NA	NA	1.28	2.13	0.06	0.81	0.62	0.76	6,736	5,184	2.54
SA34	769	BM Zone	maj	disseminated/blebby	NA	NA	0.81	2.36	0.04	NA	NA	0.06	684	4,500	0.72
SA34	772	BM Zone	mod	disseminated/blebby	NA	NA	0.79	1.70	0.04	NA	NA	NA	NA	4,444	0.80
SA34	780	BM Zone	mod	disseminated/blebby	NA	NA	0.82	1.82	0.11	NA	NA	NA	NA	2,636	0.29
SA43	764	Above BM Zone	maj	disseminated/blebby	NA	NA	0.69	2.68	0.14	NA	NA	NA	NA	5,604	2.69
SA43	769	Above BM Zone	min	disseminated/blebby	NA	NA	0.67	2.54	0.33	NA	NA	NA	NA	2,000	0.06
SA43	791	BM Zone	mod	disseminated/blebby	1.78	3.89	1.14	1.10	0.01	1.22	1.98	1.63	35,065		2.01
SA43	794	Sub-BM Zone	maj	vein	NA	NA	1.43	2.98	0.10	NA	NA	0.90	12,047	6,361	2.29

Notes: Full trace element data is available in Appendix Table A3); NA = data not available, as full 6PGE was not analyzed
Abbreviations: Alt = alteration, BMZ = Base Metal zone, maj = major, min = minimum, mod = moderate, IPGE = iridium-group platinum group element, PGE = platinum group element, PPGE = palladium-group platinum group element,

broadly correlate, showing a strong correlation in intersections of semimassive/massive sulfides (Fig. 7B); at lower Cu and Ni concentrations, peaks of Pt and Pd may be offset downward by several meters relative to Cu and Ni (Fig. 6A). The Pt/Pd ratio ranges from 0.2 to 0.7, and Pd/Ir ratios range from 0.35 to 0.73, aside from a sample from the very base of the Base Metal zone, which has a Pd/Ir ratio of 20.8 (Table 2). Peaks in Co correlate strongly with Ni and Cu (Figs. 6A, 7C), whereas Au shows a weaker correlation with PGEs, Cu, and Ni (Figs. 6A, 7D). The S/Se ratios range from 5,702 to 8,393 (Table 2).

Where the Base Metal zone is developed as disseminated/blebby sulfides (Fig. 6B), as opposed to massive sulfides (Fig. 6A), Ni/Cu ratios are generally lower (avg 2.2), whereas Pt/Pd (0.7–1.4) and Pd/Ir (1.22) ratios are higher. As with the semimassive to massive sulfides, Co, Pt, Pd, and Rh broadly correlate with Ni and Cu, whereas Au shows a weaker correlation (Figs. 6B, 7D). The S/Se ratios range from 2,000 to 6,361 (Table 2).

Cu, Ni, and PGE tenors

The concentrations of Ni, Cu and PGE in 100% sulfide (i.e., metal tenors) were calculated applying the method of Barnes and Lightfoot (2005) and are outlined in Table 3. Samples containing <0.2 wt % S were excluded from the calculations. In line with our petrographic assessment, we assume that the sulfide mineralogy is pentlandite, pyrrhotite, and chalcopyrite. The Ni tenors are variable between 5.5 and 14.3 wt %. Semimassive/massive sulfides have lower Ni tenors (4.9–9.2 wt %) than disseminated to blebby sulfides (6–14.3 wt % Ni). Copper tenors are more restricted than Ni, with all semimassive/massive sulfides having consistently low Cu tenors (0.3–1.7 wt %), whereas disseminated/blebby sulfide tenors are higher (2–7.9 wt % Cu).

Platinum, Pd, and Rh tenors are variable. Disseminated/blebby sulfides range from 4 to 153 ppm Pd, 3 to 174 ppm Pt, and 3 to 249 ppm Rh, whereas semimassive/massive sulfide tenors are more consistent from 0.9 to 2.8 ppm Pd, 0.3 to 1.8 ppm Pt, and 0.9 to 11 ppm Rh. The IPGE tenors of semimassive/massive sulfides are up to 2.2 ppm Os, 3.5 ppm Ir, and 17.3 ppm Ru. The IPGE tenors of disseminated/blebby sulfides are only available for one sample, but are significantly higher; Os, Ir, and Ru tenors are 81, 126, and 818 ppm.

Primitive mantle-normalized metal profiles

Primitive mantle-normalized whole-rock patterns for the Base Metal zone, displayed by sulfide texture, are shown in Figure 8A. The sample of disseminated/blebby sulfides shows distinctive enrichment in IPGE + Rh. It has a positive slope between Os to Rh and a steeply decreasing slope from Rh through to Au. The semimassive/massive sulfides also show enrichment in IPGEs + Rh relative to Pt, Pd, and Au, seen by an extreme negative slope from Rh through to Pt, followed by a steady increase in the profile from Pt to Cu. One semimassive/massive sulfide sample, containing the highest Cu and Ni, has a different profile to the other samples. It exhibits a positive slope from Os all the way through to Cu; however, it displays an extreme positive Rh anomaly. The overlying PGE reef in the deep Platreef at Sandsloot is plotted on Figure 8A for comparison. The Base Metal zone is anomalously low in Pt, Pd, and Au but enriched in IPGEs + Rh, compared to the PGE reef.

Downloaded from http://pubs.geoscienceworld.org/segweb/economicgeology/article-pdf/120/4/997/7306637/5159_canham+et+al.pdf
by University of the Witwatersrand user

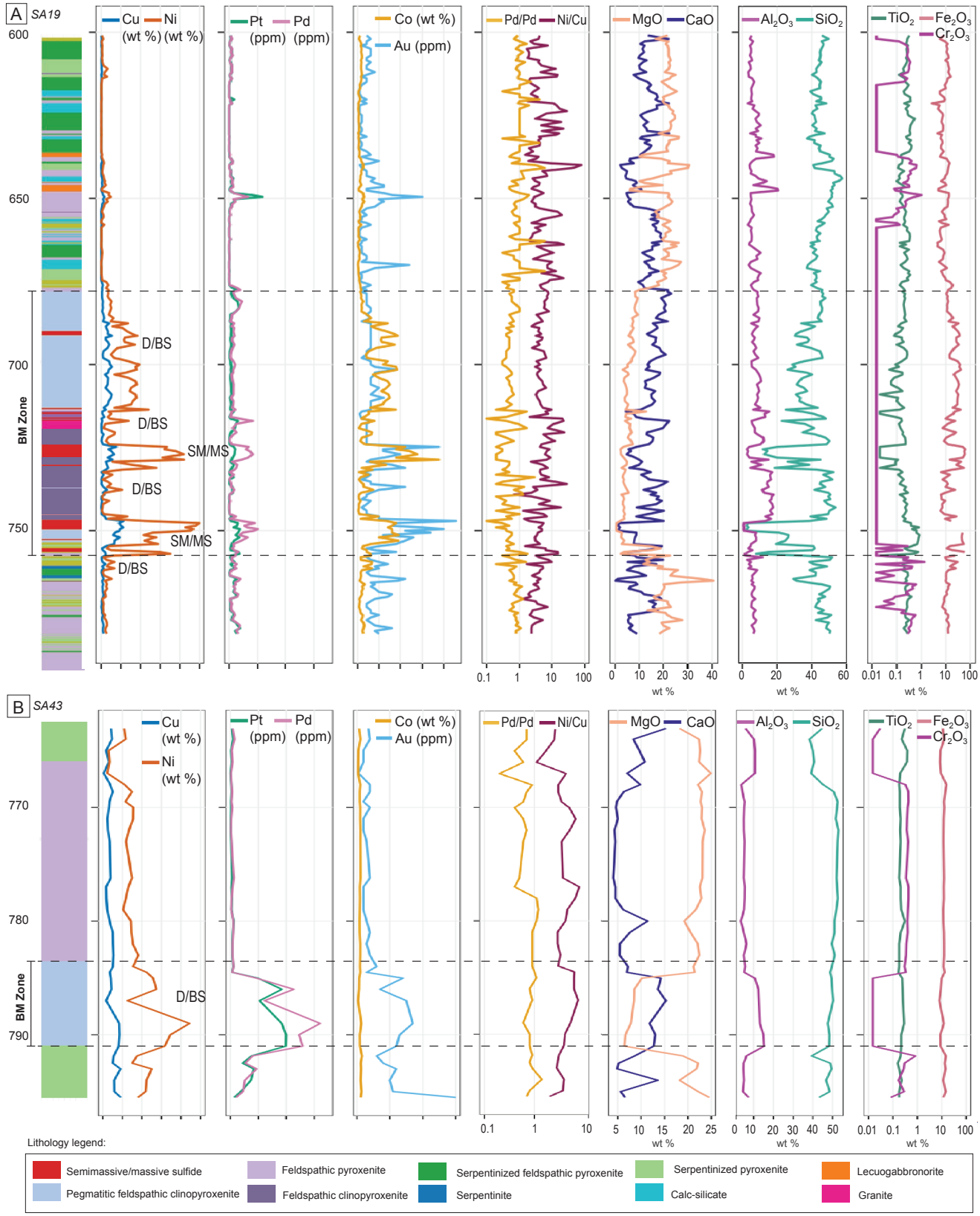

Fig. 6. Downhole stratigraphic, lithological, geochemical, and relative metal contents plots of (A) SA19 and (B) SA43 through the Base Metal (BM) zone, with the overlying Subreef and underlying Sub-Base Metal zone also shown. The Base Metal zone in (A) intersects massive/semimassive sulfides as well as disseminated/blebby sulfides, while the Base Metal zone in (B) only intersects blebby/disseminated sulfides. Geochemistry was provided by Anglo American. Abbreviations: D/BS = disseminated/blebby sulfides, SM/MS = semimassive/massive sulfides.

Downloaded from http://pubs.geoscienceworld.org/segweb/economicgeology/article-pdf/120/4/997/7306637/5159_canham+et+al.pdf
by University of the Witwatersrand user

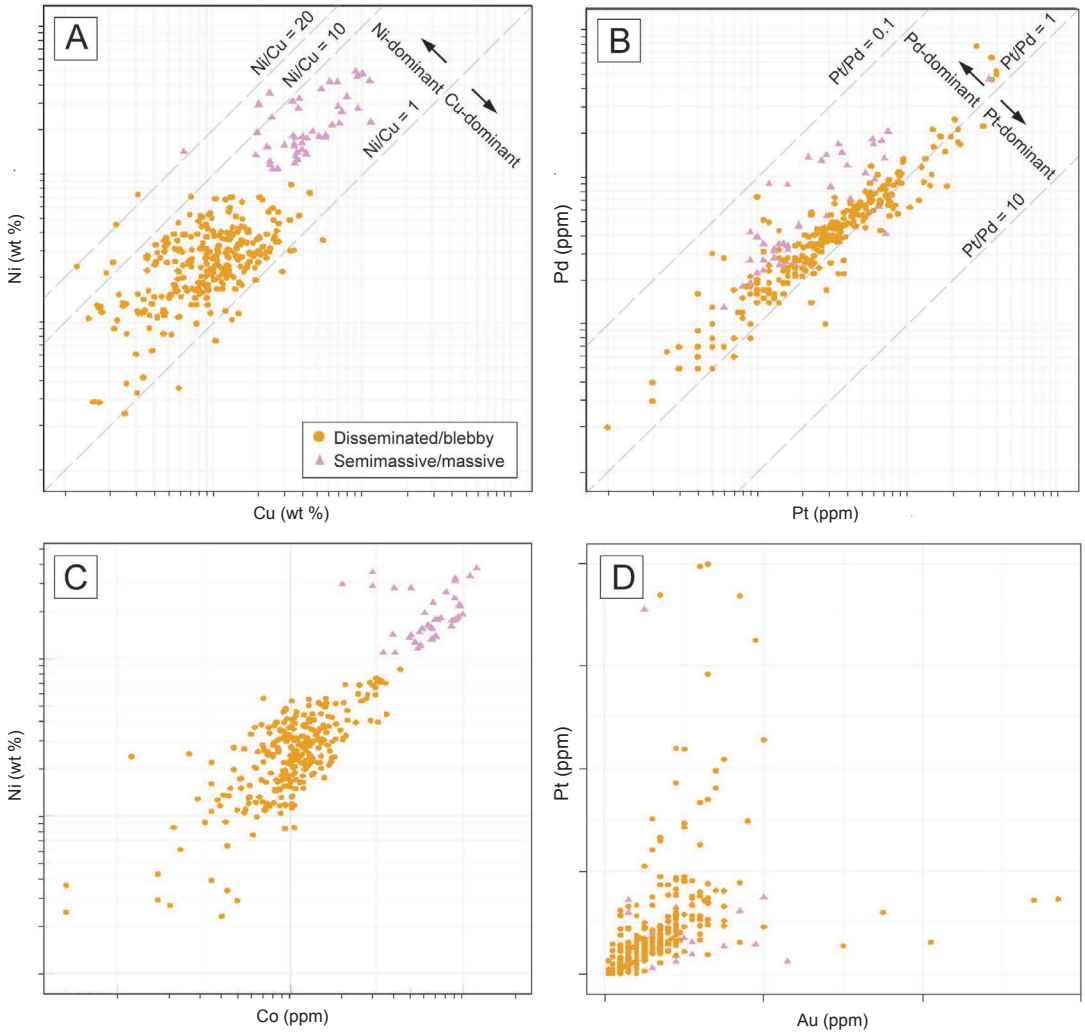

Fig. 7. X-Y plots of whole-rock chalcophile metals in the Base Metal zone in the deep Platreef at Sandsloot. (A) Cu versus Ni (logged scale), (B) Pt versus Pd (logged scale), (C) Co versus Ni (logged scale), (D) Au versus Pt. Geochemistry was provided by Anglo American.

Table 3. Cu, Ni, and PGE + Au in 100% Sulfide in the Base Metal Zone at Sandsloot

Hole ID	Sample ID	Zone	Sulfide texture	Ni wt %	Cu wt %	Pd ppm	Pt ppm	Rh ppm	Ir ppm	Os ppm	Ru ppm	Au ppm
SSAA019	SA019_705	BM Zone	Semimassive/massive	6.97	1.77	0.93	0.33	7.80	2.66	1.61	16.24	0.12
SSAA019	SA019_724	BM Zone	Semimassive/massive	4.94	0.47	2.36	0.49	7.27	NA	NA	NA	0.32
SSAA019	SA019_726A/B	BM Zone	Semimassive/massive	5.30	0.30	1.08	0.42	6.75	2.63	1.50	7.48	0.09
SSAA019	SA019_727	BM Zone	Semimassive/massive (vein)	5.62	0.26	1.28	0.52	7.51	3.01	1.50	7.51	0.15
SSAA019	SA019_729A/B	BM Zone	Semimassive/massive	6.26	0.72	2.55	1.72	11.24	3.51	2.22	17.25	0.17
SSAA019	SA019_749	BM Zone	Semimassive/massive	5.54	1.04	1.55	0.43	0.95	0.07	0.02	0.12	0.17
SSAA019	SA019_750	BM Zone	Semimassive/massive	9.24	1.65	2.76	1.76	1.04	NA	NA	NA	0.49
SSAA029	SA029_761	BM Zone	Disseminated/blebby	6.17	2.89	25.60	32.79	19.47	NA	NA	NA	1.50
SSAA034	SA034_769	BM Zone	Disseminated/blebby	10.63	4.50	52.39	42.63	3.08	NA	NA	NA	2.05
SSAA034	SA034_772	BM Zone	Disseminated/blebby	8.11	4.77	22.45	17.77	NA	NA	NA	NA	0.94
SSAA034	SA034_780	BM Zone	Disseminated/blebby	14.33	7.88	34.60	28.42	NA	NA	NA	NA	3.71
SSAA043	SA043_764	Above BM Zone	Disseminated/blebby	5.45	2.04	4.13	2.85	NA	NA	NA	NA	0.57
SSAA043	SA043_769	Above BM Zone	Disseminated/blebby	NA	NA	NA	NA	NA	NA	NA	NA	NA
SSAA043	SA043_791	BM Zone	Disseminated/blebby	7.80	7.12	153.44	174.32	249.56	126.08	81.34	818.94	2.22
SSAA043	SA043_794	Sub-BM Zone	Vein	3.88	1.30	17.39	24.82	15.71	NA	NA	NA	1.69

Notes: Calculated following the formula of Barnes and Lightfoot (2005); NA = not applicable
Abbreviations: BMZ = Base Metal zone, PGE = platinum group elements

Downloaded from http://pubs.geoscienceworld.org/segweb/economicgeology/article-pdf/120/4/997/7306637/5159_canham+et+al.pdf
by University of the Witwatersrand user

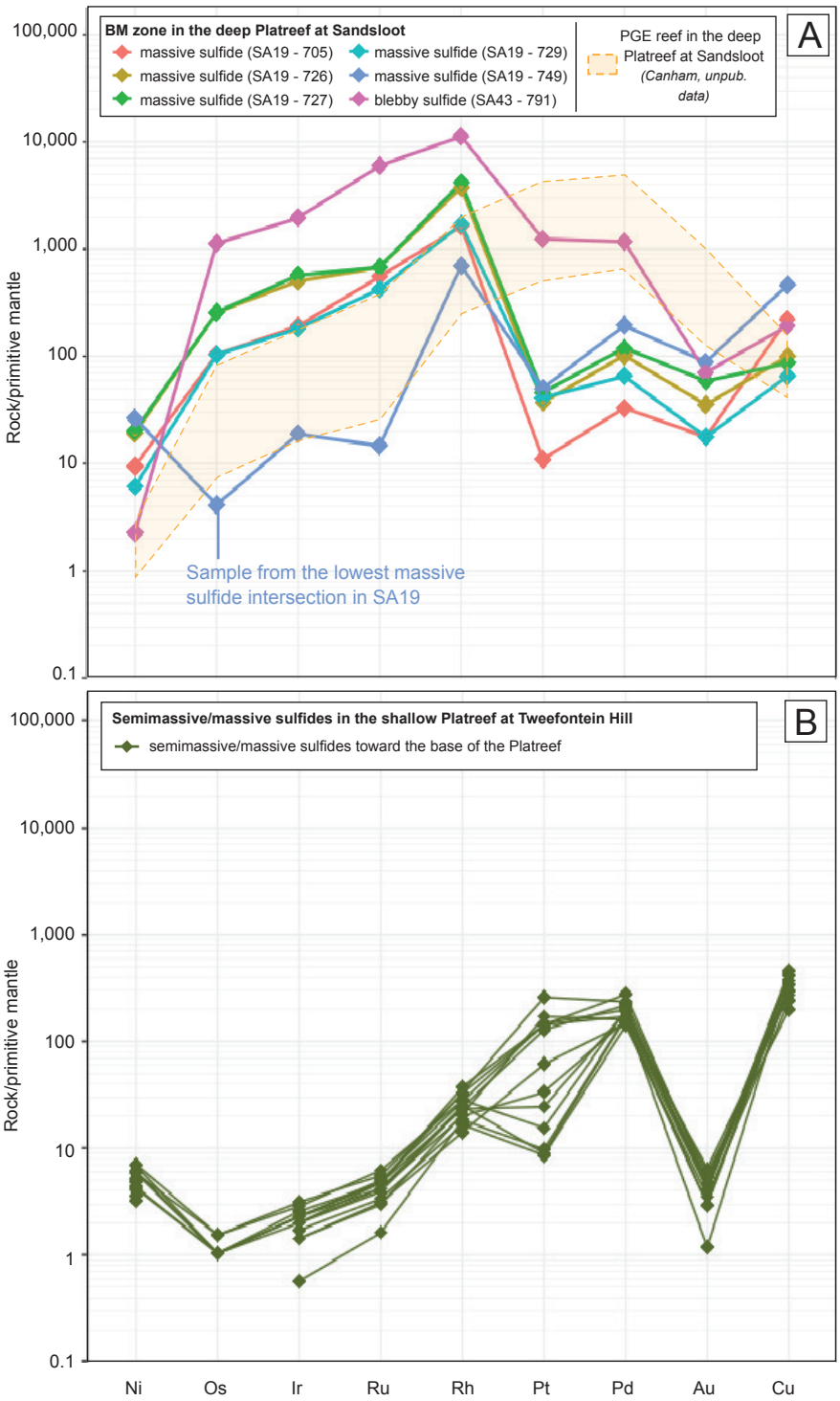

Fig. 8. Whole-rock platinum group element (PGE) + Cu + Ni normalized to primitive mantle for (A) the Base Metal (BM) zone in the deep Platreef at Sandsloot and (B) net-textured and semimassive sulfides toward the base of the shallow Platreef at Tweefontein Hill. The field for the overlying PGE reef in the deep Platreef at Sandsloot (from Canham et al., 2024, unpub. data) is also shown on (A). Primitive mantle values are from Palme and O'Neill (2014).

In Figure 8B, primitive mantle-normalized PGE patterns are shown for semimassive/massive sulfides that occur toward the base of the shallow Platreef at Tweefontein Hill (Nex, 2005). Their profile shows a positive slope from Os through to Cu, but with an extreme negative Au anomaly. Excluding the negative Au anomaly, the shape of the PGE profile at Tweefontein Hill is similar to the PGE reef in the deep Platreef at Sandsloot; however, PGE is an order of magnitude lower, while Ni and Cu are higher. When compared to the Base Metal zone, the Tweefontein Hill profile shows a posi-

Downloaded from http://pubs.geoscienceworld.org/segweb/economicgeology/article-pdf/120/4/997/7306637/5159_canham+et+al.pdf
by University of the Witwatersrand user

tive profile from Os through to Pd. In contrast, the Base Metal zone shows a positive profile from Os to Rh, followed by a very steep negative profile from Rh to Pd or Pt, which then flattens to Au. The concentrations of Ni can be significantly higher in the Base Metal zone at Sandsloot than Tweefontein Hill, while the Cu concentrations are comparable.

Trace Elements in Sulfide

Summary statistics of the trace element concentrations for the different sulfide styles and minerals are provided in Table 4. A selection of trace element contents in pentlandite and pyrrhotite is also displayed in Figure 9.

Across the sulfide styles, pentlandite generally contains the highest concentrations of Rh, Pd, and Co, while both pyrrhotite and pentlandite contain similar concentrations of Ru, Os, and Ir. Chalcopyrite generally contains no appreciable PGEs (Table 4).

When comparing the sulfide styles, blebby/disseminated sulfides contain higher Pd, Ru, and Rh in pentlandite than semimassive/massive sulfides. The Rh and Ru concentrations can reach up to 244 and 45 ppm, respectively, in blebby/disseminated pentlandite (Fig. 9A-C). In contrast, the Os and Ir concentrations of pentlandite and pyrrhotite are comparable in both disseminated/blebby and semimassive/massive sulfides (Fig. 9D, E). Semimassive/massive sulfides contain no Pt in solid solution, but notably, blebby/disseminated pentlandite can contain up to 4.2 ppm Pt (Table 4). The PGE contents in vein sulfides appear to mirror that of either the disseminated/blebby sulfide or semimassive/massive sulfide with which they are spatially associated. Two vein samples were analyzed. One sample, a sulfide-calcite vein in the Sub-Base Metal zone, has similar high Pd and Rh contents in pentlandite to overlying disseminated/blebby sulfides from the same drill hole. The second, a Cu-rich fractionated vein associated with a zone of semimassive/massive sulfides, has significantly lower Pd and Rh contents within pentlandite, comparable to the semimassive/massive sulfides with which it is spatially associated.

Platinum Group Mineralogy

A total of 240 grains of precious metal minerals, totaling 57,007 μm², were identified from the seven thin sections analyzed (Table 5; full results available in App. Tables A5 and A6). One blebby sulfide sample contained several very coarse PGMs (each >5,000 μm²); therefore, results are presented as both number of grains and relative area. Platinum-group minerals were grouped into the following categories: (1) Ru-S, (2) Ir-As, (3) IPGE + Pt-As-S, (4) Ir alloys, (5) PPGE-As, (6) Pt-Bi-Te, (7) Pd-Bi-Te, (8) Pt-Fe, and (9) Au-Ag. A summary of the PGM groups with PGM names and ideal formulas is given in Table 5.

By number of grains, Ru-S (27%), Ir-As (20%), IPGE + Pt-As-S (16%), and Au-Ag (15%) are the most common PGMs and precious metal minerals (PMMs). The Pt-Fe (9%), PPGE-As (6%), and Pt-Bi-Te (6%) are less abundant, and Pd-Bi-Te and Ir alloys constitute <1% each (Fig. 10). By % of PGM by area, Ru-S is the most dominant PGM (62%), followed by IPGE + Pt-As-S (21%), Pt-Fe (11%), and Au-Ag (3%). The Ir-As, Pt-Bi-Te, Pd-Bi-Te, Ir alloys, and PPGE-As make up <1% of PGMs by area each (Fig. 10).

The PGMs were also classified according to their association with surrounding minerals (Fig. 11A). The majority of PGMs have a close association with base metal sulfides (Fig. 11B-H). Ir-As (Fig. 11C), Ir alloys, and Pt-Pd-Bi-Te are hosted exclusively by sulfide or on sulfide boundaries. The Ru-S, IPGE + Pt-As-S, and Au-Ag are found predominately hosted within (23 to 33% of grains) or on sulfide boundaries (25–57% of grains; Fig. 11D-G). Less commonly, they are hosted within secondary silicates (10–31% of grains; Fig. 11H). Conversely, the Pt-Fe and PPGE arsenides are often hosted within secondary silicates, such as prehnite and serpentine (67% of PPGE-As and 39% of Pt-Fe grains), although a portion of these are associated with sulfide (Fig. 11A).

Mass Balance

Six samples with full bulk-rock PGE geochemistry, in situ LA-ICP-MS sulfide analyses, and PGM data available were selected for mass balance calculations. These included four semimassive/massive sulfide samples, one Cu-rich fractionated sulfide vein, and one blebby sulfide sample. To establish the percentage of each PGE contained within each sulfide (P_{Sul}^{i}), the equation of Godel et al. (2007) was utilized:

$$(P_{Sul}^{i}) = (F_{Sul} C_{Sul}^{i} / C_{WR}^{i}) \times 100$$

Where F_{Sul} is the relevant sulfide weight fraction, C_{Sul} is the concentration of the element i (either Pt, Pd, Rh, Ru, Ir, Os) in the sulfide, and C_{WR} is the concentration of the element i in the whole rock (Godel et al., 2007). Full results are available in Appendix Table A7.

Palladium is always accounted for in total sulfide, predominantly pentlandite, and this is in agreement with our PGM analysis, in which only 0.2% of the total PGM area was Pd dominant. Palladium in sulfide is slightly overestimated (ranging from 108–121%); however, overestimations have also been reported in other deposits where Pd is accounted for totally in pentlandite (e.g., Osbahr et al., 2013). In contrast to Pd, almost no Pt is contained within sulfide. All massive/semimassive sulfides contain no Pt in sulfide, while blebby sulfides can contain up to 0.7% of total Pt in pentlandite (Fig. 12).

A sample of a Cu-rich fractionated sulfide vein (Table 1) contained a lower proportion of IPGE + Rh within sulfide compared to the other semimassive/massive sulfides. Total sulfide hosts <2% of IPGE + Rh. Within the remaining semimassive/massive sulfides, the proportion of Rh contained within sulfide is variable, ranging from 19 to 64%. The Ru, Os, and Ir proportions range from 55 to 100%, 10 to 100, and 29 to 80% in total sulfide, respectively. The blebby sulfide sample only contains 3.0, 2.3, and 0.6% Ru, Os, and Ir in total sulfide, which is in agreement with the abundance of Os-Ir–bearing laurite and IPGE + Pt-As-S observed in this sample (Fig. 11E, G).

Discussion

The Base Metal zone in the deep Platreef at Sandsloot is a sulfide-rich zone that lies 50 to 150 meters beneath the PGE reef. The most important features identified in this study, which require explanation, are as follows:

1. High IPGE + Rh, resulting in (IPGE + Rh)/(Pt + Pd) ratios ranging from 0.6 to 22.4 (mean 9.6) and Pd/Ir ratios generally <1.5, as well as high Ni/Cu ratios (1.1–21.6);

Downloaded from http://pubs.geoscienceworld.org/segweb/economicgeology/article-pdf/120/4/997/7306637/5159_canham+et+al.pdf
by University of the Witwatersrand user

Downloaded from http://pubs.geoscienceworld.org/segweb/economicgeology/article-pdf/120/4/997/7306637/5159_canham+et+al.pdf
by University of the Witwatersrand user

Table 4. Summary of LA-ICP-MS Analysis of Trace Elements in Sulfide in the Base Metal Zone at Sandsloot

Sulfide texture	Mineral		^{57}Fe wt %	^{59}Co ppm	^{61}Ni wt %	^{63}Cu wt %	^{75}As ppm	^{77}Se ppm	^{101}Ru ppm	^{103}Rh ppm	^{107}Ag ppm	^{108}Pd ppm	^{121}Sb ppm	^{125}Te ppm	^{189}Os ppm	^{193}Ir ppm	^{195}Pt ppm	^{197}Au ppm	^{208}Pb ppm	^{209}Bi ppm
Diss/blebby	po	Average	59.6	30.1	0.22	0.00	*	67.1	14.4	3.62	0.25	0.08	0.18	0.49	1.46	1.53	0.14	0.14	1.72	0.06
n of samples = 3	(*n* = 12)	Min	56.2	13.7	0.10	0.00	*	53.2	0.74	*	0.08	*	*	*	0.12	0.03	*	*	0.84	*
		Max	65.5	51.9	0.33	0.01	*	85.1	42.7	20.1	0.64	0.25	0.18	0.51	4.68	4.17	0.31	0.29	2.48	0.33
		2σ	5.64	23.2	0.14	0.01	*	23.3	28.2	12.8	0.30	0.19	*	0.06	2.67	3.09	0.23	0.20	0.99	0.19
Semimassive/	po	Average	60.5	29.6	0.33	0.00	*	36.9	6.96	0.43	0.15	0.02	0.15	0.11	1.15	0.91	*	0.07	1.81	0.42
massive	(*n* = 22)	Min	55.0	21.0	0.22	0.00	*	27.7	*	*	*	*	*	*	*	0.03	*	*	0.53	0.11
n of samples = 6		Max	68.7	48.4	0.43	0.02	*	47.0	19.1	1.82	0.51	0.02	0.15	0.17	1.81	1.94	*	0.18	6.81	1.27
		2σ	6.44	16.3	0.10	0.01	*	11.8	10.1	0.91	0.28	0.01		0.18	0.83	1.38	*	0.13	2.91	0.55
Vein	po	Average	60.6	17.3	0.18	0.00	*	51.5	0.56	0.06	0.55	0.09	0.04	0.22	0.13	0.17	0.10	0.04	5.09	0.42
n of samples = 2	(*n* = 11)	Min	53.6	13.1	0.03	0.00	*	29.0	0.01	0.01	*	*	*	*	*	0.02	*	*	1.18	*
		Max	68.6	20.8	0.35	0.00	*	86.2	1.82	0.12	3.13	0.12	0.07	0.22	0.18	0.57	0.10	0.08	25.8	1.07
		2σ	11.3	5.56	0.27	0.00	*	29.1	1.36	0.08	1.85	0.08	0.04		0.09	0.42		0.08	14.2	0.73
Diss/blebby	pn	Average	31.1	10,300	28.6	0.07	1.34	65.0	23.7	116	3.05	346	0.29	1.75	2.20	2.32	2.51	0.11	10.8	0.22
n of samples = 3	(*n* = 6)	Min	30.2	9,520	23.8	0.00	0.95	55.1	0.72	4.07	1.27	74.4	*	*	0.12	0.48	0.25	*	2.99	0.01
		Max	33.2	11,100	30.3	0.34	1.93	70.8	45.0	244	4.17	657	0.67	1.75	6.81	5.23	4.22	0.22	33.3	1.22
		2σ	2.30	1,230	4.90	0.27	0.84	11.4	31.7	238	1.98	591	0.65		4.84	3.63	3.49	0.17	22.8	0.98
Semimassive/	pn	Average	32.4	11,100	31.1	0.00	0.56	34.5	8.48	12.2	1.18	10.2	*	1.59	1.24	1.59	*	0.06	4.19	0.39
massive	(*n* = 37)	Min	29.3	8,250	25.7	0.00	*	25.6	0.51	0.01	0.15	2.66	*	*	*	*	*	*	0.15	0.05
n of samples = 6		Max	37.8	13,500	37.8	0.01	1.07	50.9	23.7	62.9	4.45	21.1	*	7.93	4.53	8.15	*	0.15	14.7	1.41
		2σ	4.56	3,060	6.65	0.01	0.53	12.3	13.5	33.2	2.45	8.97	*	4.62	1.95	3.86	*	0.08	7.13	0.60
Vein	pn	Average	33.1	10,900	28.2	0.00	0.34	51.1	2.16	18.7	6.42	153	*	1.21	0.12	0.58	0.22	0.02	16.8	0.79
n of samples = 2	(*n* = 10)	Min	29.3	8,690	26.8	0.00	*	32.8	0.47	0.02	0.20	5.09	*	*	*	*	*	*	2.27	*
		Max	37.4	12,500	29.7	0.00	0.46	87.9	4.03	86.9	18.8	285	*	2.77	0.18	1.27	0.30	0.03	43.4	1.38
		2σ	6.39	3,120	1.73	0.00	0.17	34.9	2.95	52.3	12.9	254	*	2.38	0.11	0.98	0.12	0.03	30.1	1.13
Diss/blebby	cpy	Average	27.7	9.81	0.04	30.7	*	47.2	-	-	3.18	-	*	0.63	0.90	0.09	0.14	0.28	11.2	0.06
n of samples = 3	(*n* = 5)	Min	26.8	0.16	0.00	29.9	*	38.4	-	-	1.34	-	*	*	*	*	*	*	7.65	*
		Max	28.4	38.0	0.14	31.8	*	64.3	-	-	5.29	-	*	0.63	0.90	0.09	0.15	0.53	16.7	0.08
		2σ	1.41	31.9	0.11	1.39	*	22.5	-	-	3.56	-	*				0.03	0.45	7.79	0.06
Semimassive/	cpy	Average	29.8	11.0	0.04	32.3	*	32.2	-	-	1.38	-	*	0.43	0.68	0.32	*	0.07	4.46	0.47
massive	(*n* = 15)	Min	27.0	*	0.00	27.1	*	19.2	-	-	0.30	-	*	*	*	*	*	*	1.97	0.06
n of samples = 6		Max	38.1	90.0	0.23	37.6	*	41.2	-	-	2.63	-	*	0.65	1.55	1.19	*	0.15	7.09	1.23
		2σ	5.89	46.4	0.12	4.53	*	11.9	-	-	1.62	-	*	0.64	1.06	0.79	*	0.11	3.43	0.69
Vein	cpy		37.5	4.92	0.01	20.0	*	28.3	-	-	2.84	-	*	*	*	0.04	*	0.05	49.9	0.02
n of samples = 1	(*n* = 1)																			

Notes: Diss = disseminated, LA-ICP-MS = laser ablation-inductively coupled plasma-mass spectrometry, *n* = number of analyses (full results are available in App. Table. A4), * = below detection limit, - = no analysis

Mineral abbreviations: cpy = chalcopyrite, pn = pentlandite, po = pyrrhotite

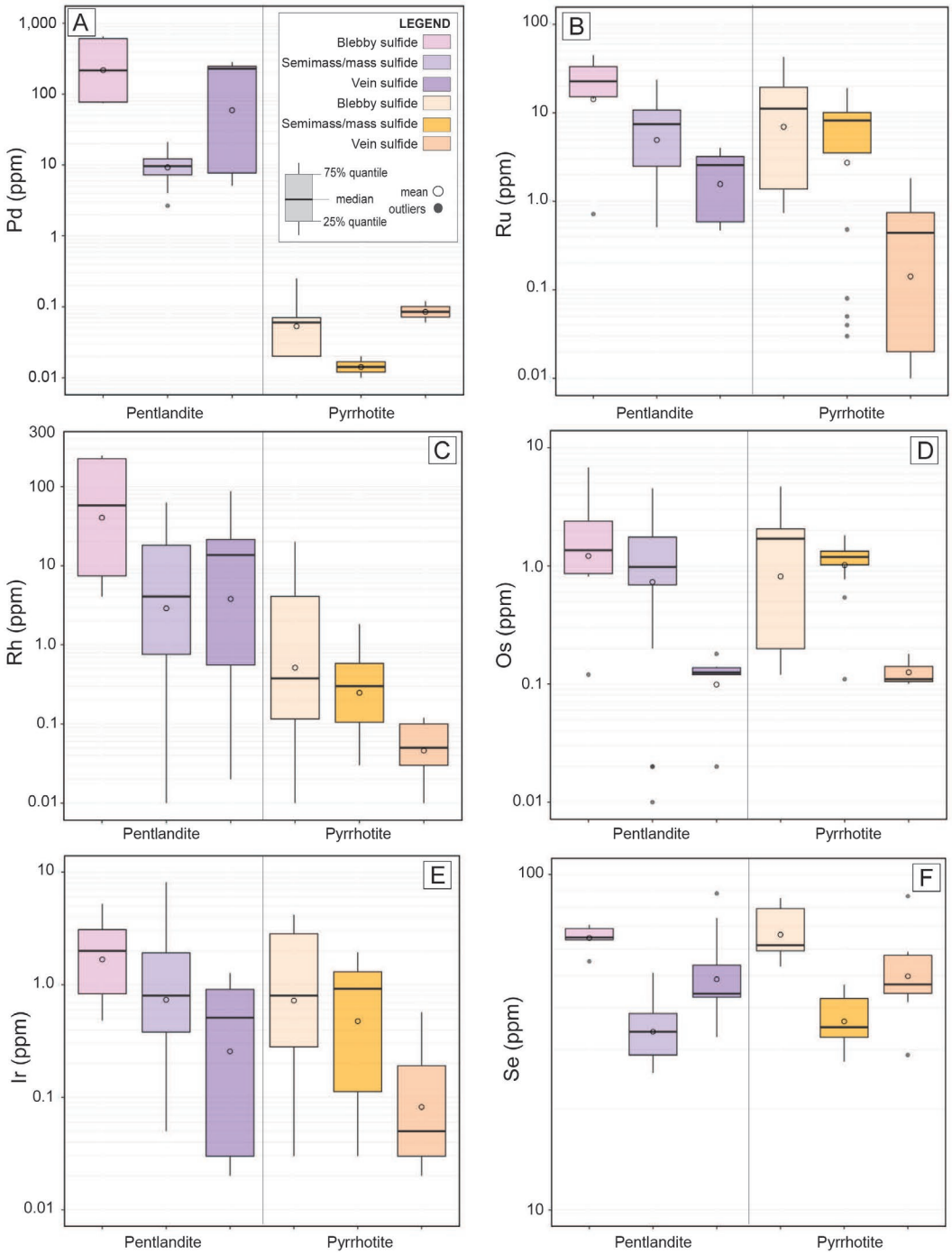

Fig. 9. Box and whisker plots of (A) Pd, (B) Ru, (C) Rh, (D) Os, (E) Ir, and (F) Se contents in pentlandite and pyrrhotite in the Base Metal zone in the deep Platreef at Sandsloot. Each box represents a different sulfide texture.

2. High but variable PGE tenors within disseminated/blebby sulfides (4–153 ppm Pd, 3–174 ppm Pt, 249 ppm Rh, 818 ppm Ru, 126 ppm Ir, 81 ppm Os), while tenors of semimassive to massive sulfides are lower but more consistent (<2 ppm Pt and Os, <3 ppm Pd, <4 ppm Ir, <12 ppm Rh, and <18 ppm Ru);
3. An almost exclusively Ir-As, IPGE + Pt-As-S, and Ru-S PGM assemblage, with minor Ir alloys, PPGE-As, Pt ± Pd-Bi-Te, Pt-Fe, and Au-Ag; and
4. Palladium hosted almost exclusively within pentlandite and Pt hosted almost exclusively by PGMs, while IPGE+Rh are hosted variably by PGMs and sulfides, apparently correlating with the volume of sulfide in the sample.

Processes controlling the formation of IPGE + Rh-dominant mineralization

The most significant finding of this study is the dominance of IPGEs + Rh compared to Pt + Pd + Au within the Base

Downloaded from http://pubs.geoscienceworld.org/segweb/economicgeology/article-pdf/120/4/997/7306637/5159_canham+et+al.pdf
by University of the Witwatersrand user

Table 5. Table Summarizing the % of PGM and PMM by Area and Number of Grains, Alongside their Total Areas and Number (*n*) of Grains

PGM group	PGM name	Ideal formula	% of PGM by total area	% of grains	Total area (μm²)	Total *n* of grains
Ru-S	Laurite	$(Os, Ir)RuS_2$	61.8	27.3	35,231	60
Ir-As	Iridarsenite	$IrAs_2$	1.2	19.5	671	43
IPGE + Pt-As-S	Hollingworthite	RhAsS	0.02	2.3	11	5
	Platarsite	(Pt,Ir,Os)AsS	21.3	5.5	12,136	12
	Irarsite	(Ir,Pt,Os)AsS	0.2	8.2	89	18
Ir-alloys	IrPbAs unknown	Ir-Pb-As	0.1	0.5	32	1
PPGE-As	Palladoarsenide	$PdAs_2$	0.03	3.2	15	7
	Sperrylite	$PtAs_2$	0.55	3.2	315	7
Pt-Bi-Te	Moncheite	$Pt(Te, Bi)_2$	0.7	6.4	377	14
Pd-Bi-Te	Merenskyite	$Pd(Te,Bi)_2$	0.2	0.9	101	2
Pt-Fe	Isoferroplatinum	Pt_3Fe Pt_2Fe	10.6	8.6	6,043	19
Au-Ag	Electrum	(Au-Ag)	3.5	14.6	1,985	32

Notes: The names and ideal formulas of platinum group minerals (PGMs) within each group are also given; full PGM and precious metal mineral (PMM) data sets are available in Appendix Tables A5 and A6

Abbreviations: IPGE = iridium-group platinum group elements, PPGE = palladium-group platinum group elements

Metal zone—a highly unusual feature for a magmatic sulfide deposit. High IPGE + Rh contents within magmatic sulfide deposits can occur through, and are related to, several different processes, including (1) chromite formation, (2) fractionation of sulfide melt, or (3) involvement of late-magmatic or hydrothermal fluids. Within the Bushveld Complex, the most well-known PGE horizons to show high (IPGE + Rh)/(Pt + Pd) ratios are the Lower Critical zone-hosted LG-1 to LG-4 chromitites (Naldrett et al., 2009). These are "chromitite-controlled" horizons with very low sulfide content, meaning PGEs were predominantly concentrated by chromite, rather than a sulfide liquid. This results in a characteristic IPGE + Rh enrichment relative to Pt + Pd + Au (Scoon and Teigler, 1994). However, this process does not explain the IPGE + Rh-dominance at Sandsloot, as the Base Metal zone lacks significant chromite. No chromitites or chromite seams have been noted, and whole-rock geochemistry shows very low Cr_2O_3 values (Fig. 6). Furthermore, PGE mineralization is clearly sulfide associated (Fig. 11A).

Alternatively, late-magmatic or hydrothermal fluids may have played a role in separating IPGE + Rh from Pt + Pd + Au. Within the Northern limb, fluid activity has been shown to be an important control on mobilizing some metals (e.g., Armitage et al., 2002; Holwell et al., 2006, 2017; Smith et al., 2014). Evidence of fluid involvement in the Base Metal zone at Sandsloot includes skarn textures (Fig. 4F), chlorite and serpentinite alteration, and carbonate veinlets (Fig. 5E-G). Platinum group minerals are also stranded in sulfide alteration halos in places (Fig. 11A, H). Under typical hydrothermal conditions, such as serpentinization and talc-carbonate alteration, Cu and Au are extremely mobile, Pd and Ni are moderately mobile, and Pt, Rh, and IPGE are far less mobile (Barnes and Liu, 2012). As such, hydrothermal mobilization can fractionate Cu, Au, and Pd from Rh and the IPGEs quite effectively. The Base Metal zone ores have Pt/Pd ratios generally <1 (avg 0.7; Fig. 7B), which are typical of most Northern limb PGE deposits (McDonald et al., 2005). If PGE had been mobilized away from the Base Metal zone, Pd would be expected to be lower than Pt due to its higher mobility. Furthermore, there are no systematic changes in other immobile/mobile element ratios, such as Rh/Pd, between the least and most heavily altered samples (Table 2). However, it is possible under highly oxidized, acidic conditions to also mobilize Pt and Ni (Barnes and Liu, 2012; Liu et al., 2012). Alternatively, more reduced fluids can mobilize Pt if there is high salinity (Sullivan et al., 2022). Where this alteration has occurred in other areas of the Northern limb, significant volumes of pyrrhotite are lost, sulfides are replaced by secondary pyrite and millerite, and IPGEs + Rh are typically hosted by secondary pyrite (e.g., Grasvally norite-pyroxenite-anorthosite member; Holwell et al., 2017). This style of mineralization is distinct to anything seen within the Base Metal zone. Therefore, an alternative explanation for the IPGE-rich nature of the Base Metal zone is required.

Sulfide liquid fractionation can be an extremely effective mechanism to physically separate Fe-Ni-Rh-IPGE MSS from Cu-Au-Pt-Pd ISS. The primitive mantle-normalized PGE plots (Fig. 8A) of both the disseminated/blebby and semimassive/massive sulfides display a pattern similar to those from Fe sulfide-rich ores, such as at the Creighton Ni-Cu-PGE

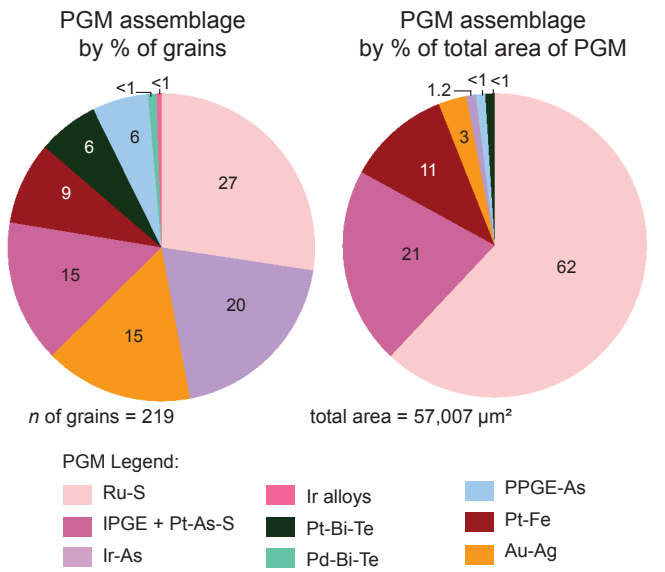

Fig. 10. Pie charts of the platinum group mineral (PGM) assemblage of the Base Metal zone in the deep Platreef at Sandsloot. Abbreviations: IPGE = iridium-group platinum group element, PPGE = palladium-group platinum group element.

Downloaded from http://pubs.geoscienceworld.org/segweb/economicgeology/article-pdf/120/4/997/7306637/5159_canham+et+al.pdf
by University of the Witwatersrand user

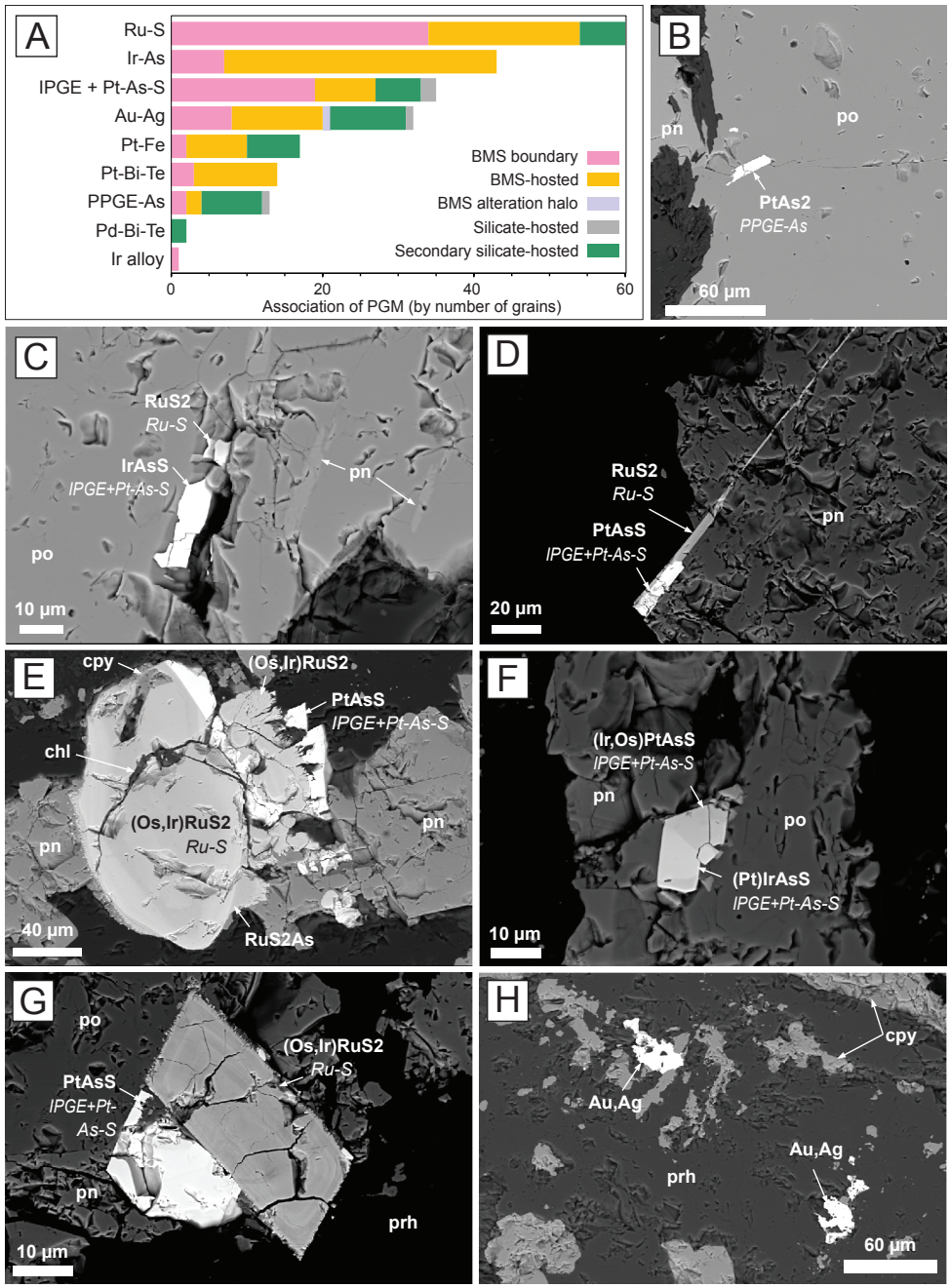

Fig. 11. (A) Stacked bar chart of the association of each platinum-group mineral (PGM) type in the Base Metal zone in the deep Platreef at Sandsloot and (B-H) photomicrographs of typical PGM textures. The formula of the PGM is given in bold and its associated PGM group is given underneath in italics. (B) $PtAs_2$ hosted in pyrrhotite. (C) IrAsS and RuS_2 hosted within pyrrhotite containing pentlandite flames. (D) Bladed PtAsS and RuS_2. (E) Coarse-grained zoned Os, Ir-bearing RuS_2, and PtAsS hosted on boundary of pentlandite; chlorite (chl) crosscuts the PGM. (F) PtAsS and Pt-bearing IrAsS within sulfide. (G) PtAsS and euhedral oscillatory zoned Os; Ir-bearing RuS_2 on sulfide prehnite boundary. (H) Electrum (Au, Ag) associated with chalcopyrite within prehnite altered plagioclase. Abbreviations: BMS = base metal sulfide, cpy = chalcopyrite, IPGE = iridium-group platinum group elements, pn = pentlandite, po = pyrrhotite, PPGE = palladium-group platinum group element, prh = prehnite.

deposit, Sudbury, and the Western Jinchuan Intrusion, northwest China (Dare et al., 2010a; Chen et al., 2013). In these deposits, the IPGE-rich profiles are thought to represent the Fe-rich monosulfide solid solution portion of a cooled and fractionated sulfide liquid, which is associated with the process of partitioning of Os, Ir, Ru, and Rh into monosulfide solid solution, while Pt, Pd, and Au go into the residual Cu-rich liquid. Upon further cooling, this Cu-rich liquid forms intermediate solid solution (Li et al., 1996; Barnes et al., 1997). This provides an effective mechanism to produce the IPGE + Rh-dominant sulfide in the Base Metal zone. However, if the Base Metal zone is representative of the monosulfide solid

Downloaded from http://pubs.geoscienceworld.org/segweb/economicgeology/article-pdf/120/4/997/7306637/5159_canham+et+al.pdf
by University of the Witwatersrand user

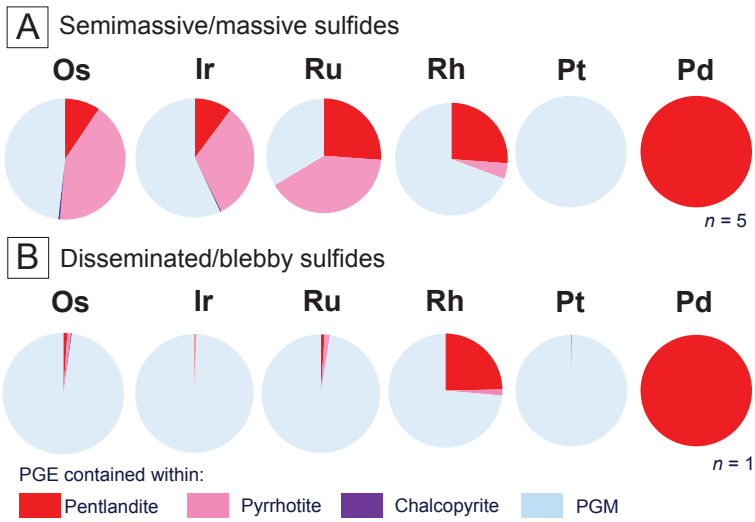

Fig. 12. Pie charts summarizing mass balance of platinum group elements (PGEs) held contained within sulfide and platinum group minerals (PGMs) within (A) semimassive/massive sulfides and (B) disseminated/blebby sulfides in the Base Metal zone in the deep Platreef at Sandsloot. *n* = number of samples.

solution portion of a sulfide liquid, this leaves a mass balance problem. Specifically, to explain the concentrations of Ni-IPGE + Rh observed, there must be significant Cu-Pt + Pd + Au elsewhere.

It is known that between 900° and 800°C, monosulfide solid solution crystallizes, separating a residual Cu-rich liquid (Kitakaze and Sugaki, 2004; Kitakaze et al., 2016). This residual liquid has the potential to migrate away from monosulfide solid solution on a variety of scales (e.g., Blanks et al., 2022). In the Base Metal zone, this process is observed on a mm to cm scale, where chalcopyrite has migrated to the boundaries of the symplectite semimassive sulfides and into the surrounding silicates (Fig. 4C), as well as through fractionated sulfide veins (Figs. 4D, 5F-G). However, this phenomenon can occur on a much larger, deposit-wide scale. Multiple examples of deposit scale separation of a Cu(+ Pt + Pd + Au)-rich liquid from Fe-rich monosulfide solid solution exist. These include the Jinchuan Intrusion, northwest China (Chen et al., 2013); the McCreedy East (Dare et al., 2014) and Rathbun deposits (Kawohl et al., 2020), Sudbury Igneous Complex, Canada; the Munali Ni-Cu-PGE deposit, Zambia (Blanks et al., 2022); and the Sakatti Cu-Ni-PGE deposit, north Finland (Brownscombe et al., 2015). Although no Cu-rich sections have yet been identified in the Base Metal zone, it is intriguing that samples from the very base of the Base Metal zone are more Cu rich and exhibit a more positive primitive mantle-normalized PGE profile (Fig. 8A). This suggests a higher proportion of intermediate solid solution relative to monosulfide solid solution, differing from the rest of the Base Metal zone. This profile is similar to those from intermediately fractionated sulfides that occur at the Eagle Ni-Cu deposit, United States (Ding et al., 2012). Further support for this interpretation is provided by Rh/Cu ratios plotted downhole. Since Rh is highly compatible within monosulfide solid solution, while Cu is highly incompatible in monosulfide solid solution (and conversely highly compatible in intermediate solid solution), Rh/Cu ratios can be used to establish the degree of fractionation of a sulfide liquid as essentially a proxy for monosulfide solid solution/intermediate solid solution (Naldrett et al., 1999, 2000). The Rh/Cu ratio decreases with depth through SA19, with the lowest Rh/Cu ratios observed in the samples from the deepest intersection (Fig. 13). The presence of intermediately fractionated PGE profiles toward the base of the Base Metal zone suggests that Cu-rich residual liquids, enriched in the missing Pt, Pd, and Au, were mobilized farther downward. To date, footwall rocks have not been intersected to the deep Platreef at Sandsloot; thus, an undiscovered Cu-Pt-Pd–rich zone at depth or downdip remains a possibility.

The steepness of the negative PGE slope from Rh through Au in the Base Metal zone at Sandsloot (Fig. 8A) is significantly more extreme than any of the other IPGE-dominant deposits (e.g., Creighton Ni-Cu-PGE deposit, Sudbury and Western Jinchuan Intrusion, northwest China; Dare et al., 2010b; Chen et al., 2013). This indicates there may be an additional control on the extreme enrichment of IPGEs + Rh relative to Pt + Pd + Au. While sulfide liquid fractionation can effectively separate Cu and Ni sulfide, it is important to note that the Cu-rich veins and zones, where it appears Cu sulfide has migrated, are associated with calcite (Figs. 3E, 5E-G). An association between carbonate and sulfide, including Cu-rich sulfides, has been noted in several Ni-Cu-PGE deposits (e.g., Blanks et al., 2022; Cherdantseva et al., 2023). Thompson et al. (2025a) and Thompson et al. (2025c) describe the Base Metal zone as a skarn-like system, based on geochemical signatures from major elements. Therefore, given the close association of calcite with Cu sulfide, it raises the possibility that some of the missing Pt + Pd + Au may have been mobilized from the orebody by metasomatic fluids rather than, or in addition to, a pure sulfide fractionation process. Thompson et al. (2025c) show the silicate mineralogy in the Base Metal zone to be skarn-like, with pegmatoidal textures, high prehnite volumes (Fig. 4C, F), and high An contents in plagioclase, alongside Niggli numbers that trend toward skarn assemblages (Thompson et al., 2025a).

It is notable, however, that sulfide veins, which show a separation of Cu and Ni (Fig. 4D) and can be associated with

Downloaded from http://pubs.geoscienceworld.org/segweb/economicgeology/article-pdf/120/4/997/7306637/5159_canham+et+al.pdf
by University of the Witwatersrand user

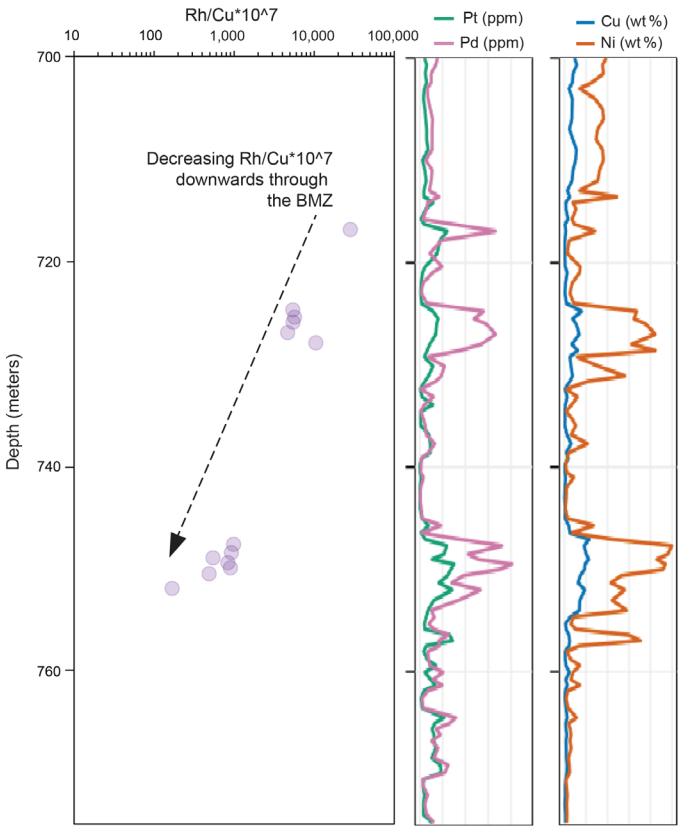

Fig. 13. Vertical profiles downhole of SA19 through the Base Metal zone (BMZ), showing the variation of Rh/Cu*10^7 with depth. The variation of Ni, Cu, Pt, and Pd downhole is also shown for reference.

carbonate (Fig. 5D, E), contain comparable Pd contents in pentlandite to the disseminated/blebby or semimassive/massive sulfides with which they are spatially associated. If Pd (alongside Cu + Pt + Au) had been lost from the Base Metal zone through metasomatic fluid interaction, it would be expected that Pd contents of pentlandite should vary between vein sulfides and the other sulfide textures. Furthermore, an abundance of low-temperature PGM species should be present if fluids mobilized Pt + Pd + Au, which are not recorded. Therefore, while skarn-like processes appear to have affected the silicate mineralogy, we do not consider this process to be the main driver for the Cu + Pt + Pd-Au–poor nature of the Base Metal zone and consider the separation of Cu and Ni sulfide to be a magmatic feature related to fractional crystallization of a sulfide liquid.

Processes controlling sulfide tenor variations

There is a clear difference in the PGE tenors between the semimassive/massive sulfides and the disseminated/blebby sulfides (Table 3; Fig. 14A). A number of different factors can influence PGE tenors, such as different degrees of fractionation, R-factor (the ratio of sulfide liquid to silicate magma), fluid involvement, and the addition of crustal S (Queffurus and Barnes, 2015).

Under low-temperature hydrothermal conditions (<300°C), S is typically far more mobile than PGEs. This means hydrothermal alteration can act to increase sulfide tenors by removing S, reducing the volume of sulfide without removing

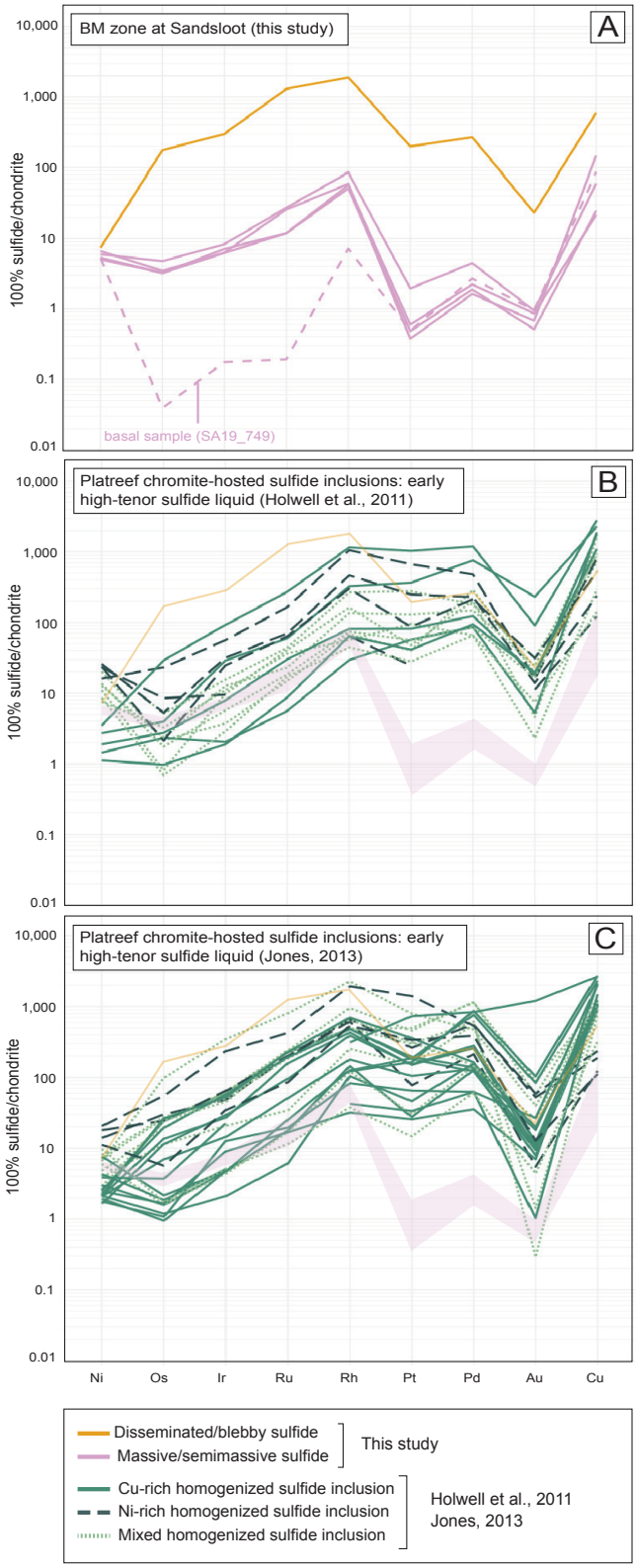

Fig. 14. Chondrite-normalized Cu, Ni, and platinum group element (PGE) tenor (Ni, Cu, and PGEs in 100% sulfide) diagrams for the (A) Base Metal (BM) zone (this study) compared to (B and C) homogenized chromite-hosted sulfide inclusions from the shallow Platreef (taken from Holwell et al., 2011; Jones 2013). The chromite-hosted sulfide inclusions have been divided into Cu-rich, Ni-rich, and mixed inclusions. Chondrite values are from Fischer-Gödde et al. (2010).

Downloaded from http://pubs.geoscienceworld.org/segweb/economicgeology/article-pdf/120/4/997/7306637/5159_canham+et+al.pdf
by University of the Witwatersrand user

the PGEs and leading to PGE enrichment (Queffurus and Barnes, 2015; Smith et al., 2016). Although there is minor alteration of sulfide around their boundaries in the Base Metal zone (Fig. 4C), tenors should vary dependent upon the degree of alteration if hydrothermal activity were responsible. However, tenors do not show this variation. Instead, they vary depending upon whether sulfides are semimassive/massive or disseminated/blebby. This suggests that either variable R-factors or involvement of crustal S are more likely controls.

In zones of semimassive/massive sulfides, where large amounts of sulfide have accumulated, the sulfide liquid is present with a low ratio of sulfide liquid to silicate magma. As a result, R-factors and metal tenors would be lower compared to the rest of the Base Metal zone, where droplets may have equilibrated with a greater volume of magma (thus producing higher R-factors). Variations in R-factor also have an influence on Se contents, meaning S/Se ratios should decrease with increasing R factor. Therefore, the highest tenor sulfides should have the lowest S/Se ratios (Thériault et al., 1997). The S/Se ratios are higher (avg = 7,536) within semimassive/massive sulfides than disseminated/blebby sulfides (avg = 4,390), providing support for the differences in sulfide tenors being an R-factor effect.

An alternative explanation to R-factor being the key control on sulfide tenors is the addition of crustal S. The initial sulfide liquid may have been very high tenor, but locally, crustal S was assimilated, essentially diluting the sulfides to lower tenors. This process would also increase the S/Se ratios. Therefore, the observed differences in S/Se ratios and PGE tenors between the different sulfide styles can alternatively be explained through this process. The disseminated/blebby sulfides represent an initial high-tenor sulfide liquid, while semimassive/massive sulfides represent high-tenor sulfides diluted by crustal S. Given that the Malmani Subgroup dolomite, a likely source of crustal S (Buchanan et al., 1981; Buchanan and Rouse, 1984), forms the footwall of the shallow Platreef at Sandsloot, we favor this mechanism over differences in R-factor. Support of this is provided by Thompson et al. (2025a) and Thompson et al. (2025c), who describe the extensive interaction of the Base Metal zone with the Malmani Subgroup sediments, which are known to contain S-bearing anhydrite layers (Buchanan and Rouse, 1984).

Though the IPGE sulfide tenors in the Base Metal zone are unusually high, very high sulfide tenors (up to 45 ppm Os, 147 ppm Ir, 506 ppm Ru, 296 ppm Rh, 1,239 ppm Pt, 683 ppm Pd) have also been reported by Holwell et al. (2006) and Jones (2013) from chromite-hosted homogenized sulfide inclusions in the shallow Platreef. As these inclusions are trapped within the earliest crystallizing phase, chromite, they are believed to represent an early high-tenor parental sulfide liquid to the Platreef. In Figure 14, the PGE tenors of the chromite-hosted inclusions are compared to those of the Base Metal zone. The chromite-hosted inclusions are divided into Ni-rich, which essentially represent a monosulfide solid solution-dominant portion of the sulfide liquid; Cu-rich, which represent an intermediate solid solution-dominant portion of the sulfide liquid; and inclusions that are mixtures of both monosulfide solid solution and intermediate solid solution. As expected, the Base Metal zone has chondrite-normalized PGE profiles that are most similar to the Ni-rich homogenized inclusions, although the depletion in Pt + Pd + Au is far more extreme in the Base Metal zone. However, what is most striking is the Base Metal zone has IPGE tenors that overlap with (in the case of massive/semimassive sulfides) or are higher than (in the case of disseminated/blebby sulfides) the chromite-hosted sulfide inclusions (Fig. 14). Since the Base Metal zone represents only the monosulfide solid solution portion of the sulfide liquid, if the Pt + Pd + Au tenors were to be extrapolated to also include the intermediate solid solution portion of the sulfide liquid (i.e., the parental sulfide liquid) the Pt + Pd + Au tenors would overlap with, or indeed exceed, those of the chromite-hosted sulfide inclusions presented by Holwell et al. (2011) and Jones (2013).

This finding has broader implications for the genesis of Platreef mineralization. Several authors have suggested that the initial sulfide liquid of the Platreef was already highly enriched in PGE prior to emplacement (e.g., McDonald and Holwell, 2007; Holwell et al., 2011), with crustal S diluting tenors on a localized scale (e.g., Sharman-Harris et al., 2005; Holwell et al., 2007; Ihlenfeld and Keays, 2011). Others (e.g., Buchanan and Rouse, 1984; Grobler et al., 2019; Maier et al., 2021; 2023) have proposed the sulfide liquid was upgraded to high tenors during magma emplacement. The IPGE tenors within the Base Metal zone are higher than any elsewhere in the Platreef and are comparable to the very high tenor chromite-hosted sulfide inclusions reported by Holwell et al. (2011) and Jones (2013), which are thought to represent a trapped early high-tenor parental sulfide liquid. Thus, this could support the idea that the Base Metal zone is representative of (at least a monosulfide solid solution portion of) that initial, high-tenor sulfide liquid. The location of the Base Metal zone downdip and west of the shallow Platreef is perhaps intriguing in this regard, as it has been proposed previously by McDonald et al. (2009) and Yudovskaya et al. (2011) that a high-grade feeder zone may be located downdip and west of the shallow Platreef at Sandsloot.

To generate such high PGE tenors prior to emplacement, a staging chamber model has been proposed (e.g., McDonald and Holwell, 2007; McDonald et al., 2009). In this model, sulfide droplets are formed and enriched with metals in a high–R-factor environment within a deep-seated staging chamber prior to magma emplacement. These sulfides are then entrained during Platreef magma ascent (Holwell et al., 2007; Smith et al., 2016). Based on the comparable tenors of the chromite-hosted sulfide inclusions and Base Metal zone sulfides, we favor this model of PGE enrichment.

Sulfide and PGM crystallization history

Figure 15 presents a schematic representation of the crystallization history and PGE behavior as the Base Metal zone formed and cooled. In an S-rich, alloy-poor system such as the Base Metal zone, IPGEs + Rh are highly compatible within monosulfide solid solution. Therefore, they are usually contained within pentlandite and pyrrhotite (Fleet et al., 1993; Li et al., 1996; Barnes et al., 1997; Mungall et al., 2005; Mansur et al., 2021). However, in the Base Metal zone, the proportion of IPGEs contained within sulfide is variable (Fig. 9B-E), with significant IPGEs also contained within PGM arsenide, arsenosulfides, and sulfide phases (Figs. 10, 11), such as Os + Ir-bearing laurite, irasite, and iridarsenite. Through experi-

Downloaded from http://pubs.geoscienceworld.org/segweb/economicgeology/article-pdf/120/4/997/7306637/5159_canham+et+al.pdf
by University of the Witwatersrand user

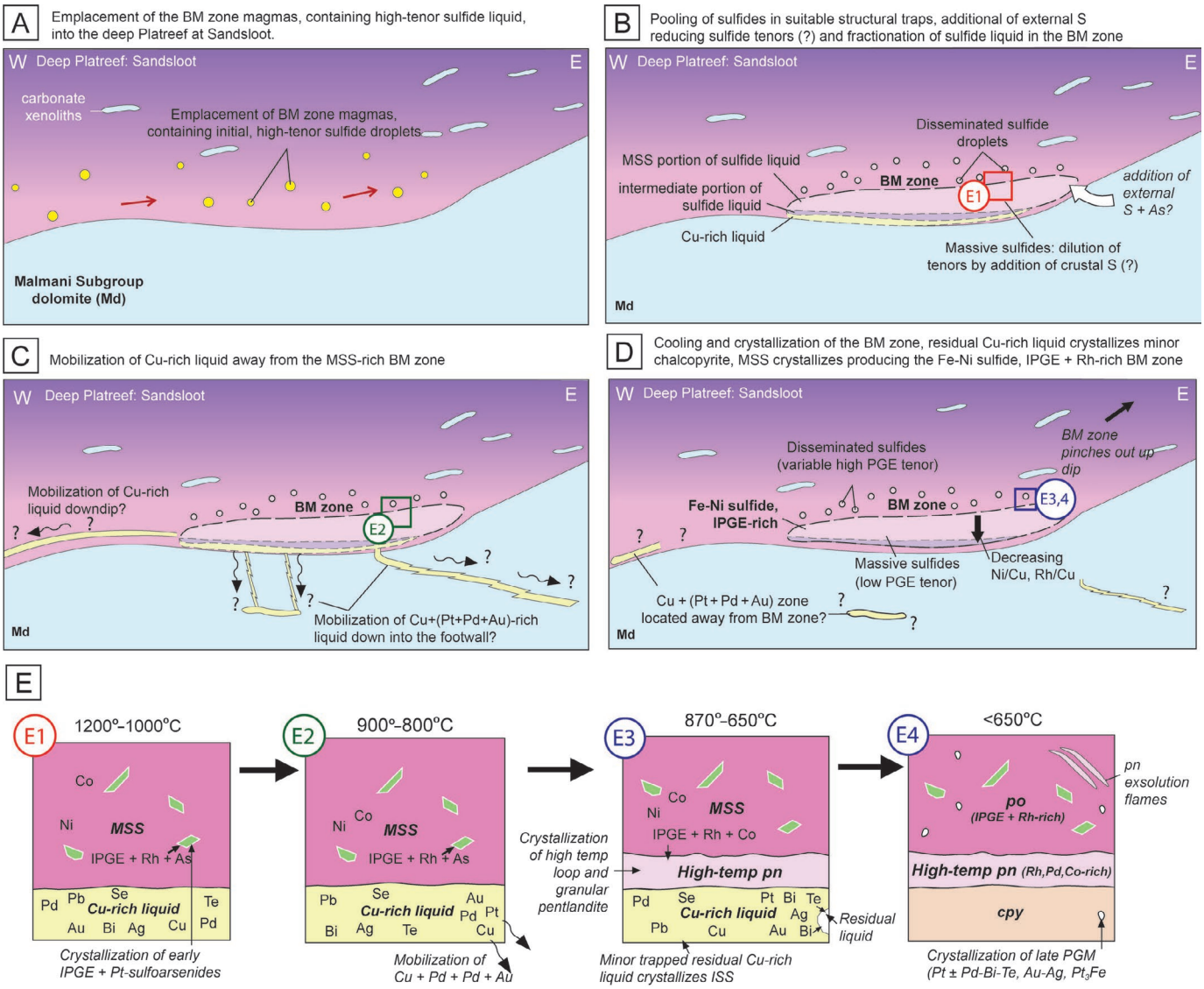

Fig. 15. Schematic illustration depicting the processes of sulfide fractionation in the formation of platinum group minerals (PGMs) and sulfides within the Base Metal (BM) zone in the deep Platreef at Sandsloot. (A-D) Illustrate the emplacement of a high-tenor sulfide liquid into the deep Platreef. This subsequently fractionates and produces the Base Metal zone, which is representative of the monosulfide solid solution (MSS) portion of the sulfide liquid. The sulfide liquid fractionated downward through the Base Metal zone and the residual Cu(+ Pt-Pd-Au)-rich liquid was likely mobilized downwards and away. (E) Shows the crystallization history of the sulfide liquid, including (E1) formation of high-temperature iridium-group platinum group elements (IPGEs) + Pt sulfoarsenides; (E2) separation of the Cu-rich liquid from monosulfide solid solution; (E3) formation of high-temperature pentlandite via peritectic reaction, and finally; (E4) low-temperature exsolution of pyrrhotite (po) and minor pentlandite (pn) from MSS and minor chalcopyrite (cpy) from intermediate solid solution (ISS).

mental studies, Helmy and Bragagni (2017) demonstrated that the formation of IPGE + Pt sulfoarsenides is highly dependent upon the activity of As within a system, which in turn is strongly controlled by S fugacity (f_{S_2}). When f_{S_2} is lowest, around 1,100°C, As is moderately compatible within the early crystallizing monosulfide solid solution (Helmy et al., 2010, 2013; Helmy and Bragagni, 2017; Piña et al., 2020). As a result, IPGEs + Pt can form early, high-temperature PGE sulfoarsenides directly from the sulfide melt (Dare et al., 2010a; Chashchin et al., 2021). The often euhedral, sulfide-hosted nature of the PGE sulfoarsenides in the Base Metal zone (e.g., Fig. 11) is consistent with their formation before crystallization of monosulfide solid solution (Liang et al., 2019). At these high temperatures, the strong affinity of As to complex Ir and Pt promotes crystallization of Ir and Pt arsenosulfides, whereas Os and Ru have a stronger affinity for S than As, forming Ru(Os) sulfides (Fig. 15E1; Helmy and Bragagni, 2017). This is entirely consistent with the PGM mineralogy we observe at Sandsloot (Figs. 10, 11), and we therefore propose that most of the IPGEs-PGMs formed in this way (Fig. 15E1). High-temperature Ir, Pt, Ru ± Os PGMs have also been described in the Creighton Ni-Cu-PGE deposit, hosted within early monosulfide solid solution cumulates (Dare et al., 2010a), analogous to those we describe at Sandsloot. Our

Downloaded from http://pubs.geoscienceworld.org/segweb/economicgeology/article-pdf/120/4/997/7306637/5159_canham+et+al.pdf
by University of the Witwatersrand user

mass balance highlights only up to 64% of the Rh is accounted for in sulfide. However, few Rh-bearing PGMs were identified in the PGM analysis, suggesting Rh PGMs may have been missed from the PGM analysis due to nugget effects. Given the abundance of irasite and platarsite, any missing Rh PGMs may be present in the form of hollingworthite, which belongs to the same solid solution series.

Unlike IPGEs + Pt, Pd does not form high-temperature semimetal complexes with As or S (Helmy et al., 2010, 2013; Helmy and Bragagni, 2017) and, therefore, will have stayed within the sulfide liquid after the formation of high-temperature Os-Ir-Ru-Rh-Pt PGMs. The IPGEs + Rh, as well as Co, are highly compatible within monosulfide solid solution, so any IPGEs + Rh that did not form the early arsenosulfide PGMs, along with Co, entered monosulfide solid solution (Li et al., 1996; Barnes et al., 1997; Mungall et al., 2005; Mansur et al., 2021). Monosulfide solid solution subsequently crystallizes pentlandite and pyrrhotite at lower temperatures; however, pentlandite formation can also occur at high temperatures (Kitakaze et al., 2016). Several authors (e.g., Dare et al., 2010a; Mansur et al., 2019; Barnes et al., 2020) have highlighted that pentlandite textures can provide insight into the crystallization history of sulfide liquids. Within the massive/semimassive sulfides, loop-textured pentlandite around pyrrhotite (Fig. 4C) and contact pentlandite between chalcopyrite and pyrrhotite (Fig. 4B) are present, whereas within disseminated/blebby sulfides, granular pentlandite occurs around pyrrhotite boundaries (Fig. 5A, B). Work by Barnes et al. (2020) and Mansur et al. (2019) shows that these pentlandite textures are products of high-temperature peritectic reaction. Kitakaze et al. (2016) experimentally demonstrated that this reaction occurs between 740° and 870°C, between early crystallized monosulfide solid solution and residual Pd-rich sulfide liquid, producing Pd-rich pentlandite. In contrast, lower-temperature exsolution pentlandite is typically Pd poor (e.g., Barnes et al., 2020). The findings that almost 100% of Pd is contained within pentlandite (Fig. 12) and that Pd contents of pentlandite can be high (Fig. 9A), along with the presence of peritectic sulfide textures (Fig. 4B, C), are all consistent with formation of pentlandite at high temperatures that incorporated Pd, as well IPGEs + Rh + Co (Fig. 15E3).

Conversely to IPGEs + Rh, Pt + Pd + (Au + Ag + Bi + Te) are highly incompatible within monosulfide solid solution, as well as intermediate solid solution (Dare et al., 2014; Liu and Brenan, 2015; Mansur et al., 2020, 2021). Therefore, Pt + (Au + Ag + Bi + Te), alongside any Pd not incorporated by high-temperature pentlandite, were concentrated into a semimetal-rich residual liquid (e.g., Helmy et al., 2010; Liu and Brenan, 2015; Mansur et al., 2020). This liquid would have crystallized Pt ± Pd-Bi-Te PGMs and Au-Ag below 650°C (Fig. 15E4). However, the relative concentrations of semimetal to Pd were low, as Pd was almost entirely taken up by high-temperature pentlandite rather than remaining in the residual sulfide liquid (Holwell and McDonald, 2010). Below 650°C (Kelly and Vaughan, 1983), pyrrhotite and pentlandite crystallized from monosulfide solid solution. Both phases subsequently trapped IPGEs and Co. Minor exsolution of pentlandite from monosulfide solid solution produced the flames-textured pentlandite observed in pyrrhotite (Figs. 4B, 15E4). As discussed above, Cu-rich sulfide liquid may have separated from the main monosulfide solid solution mass preserved in the Base Metal zone. It likely migrated downdip or into the footwall rocks (Fig. 15E2), crystallizing first intermediate solid solution and then chalcopyrite (Kelly and Vaughan, 1983).

Comparison of the Base Metal zone to sulfide-rich intersections in the wider Platreef

Throughout the Northern limb, massive sulfides are sporadically developed toward the base of the shallow Platreef. These have been attributed to downward percolation and ponding of Platreef sulfide based on their distribution in structural traps (e.g., Turfspruit and Macalaskop: Hutchinson and Kinnaird, 2005; Tweefontein Hill: Nex, 2005). Thompson et al. (2025a) and Thompson et al. (2025c) suggest that the Base Metal zone in the deep Platreef at Sandsloot formed in a similar manner, through slumping and accumulation of sulfide toward the Platreef's base. In Figure 8, primitive mantle-normalized PGE profiles of the Base Metal zone are compared to net-textured and semimassive sulfides present at the base of the shallow Platreef at Tweefontein Hill (Fig. 1). The PGE profiles of the Tweefontein Hill semimassive sulfides are more akin to that of typical Platreef than the Base Metal zone, i.e., not monosulfide solid solution-like. Additionally, the PGM assemblage at Tweefontein Hill is dominated by Pt-Pd-Bi-Te (Martin, 2018), rather than any IPGE-rich PGM as seen in the Base Metal zone. As suggested previously by Nex (2005), the PGE profiles and PGM assemblages support that the Tweefontein Hill semimassive sulfides represent accumulations of Platreef sulfide. Other reported occurrences of massive sulfides at the base of the shallow Platreef (e.g., Turfspruit and Macalacaskop: Hutchinson and Kinnaird, 2005) are characterized by significant proportions of chalcopyrite, and as such do not represent monosulfide solid solution. Therefore, while the Base Metal zone shares a similar stratigraphic location to other occurrences of semimassive/massive sulfides in the Platreef, there are clear geochemical and mineralogical differences.

Though IPGEs + Rh-rich ores have not been reported in other occurrences of sulfide-rich ores in the Bushveld, Ir-Rh-Ru–rich PGMs have been noted in the deep Platreef at Akanani, downdip from the Zwartfontein pit (Fig. 1A). It is thought these PGMs represent an early assemblage that crystallized at high temperatures; however, this assemblage is found in harzburgites, which are much poorer in sulfide than the Base Metal zone. Additionally, despite the abundance of Ir-Rh-Ru–rich PGMs, mineralization is still Pt-Pd dominant rather than IPGE-Rh dominant (Yudovskaya et al., 2011). This makes it distinct from the Sandsloot Base Metal zone.

What is apparent from the aforementioned comparisons is the Base Metal zone is not simply the monosulfide solid solution portion of the sulfide liquid from the overlying PGE reef, and appears to be a distinct sulfide generation. Additionally, the Base Metal zone appears to become more fractionated with depth, suggesting if an intermediate solid solution portion were to exist, this should be beneath the Base Metal zone rather than above where the PGE reef is located. This leaves three possibilities: either (1) the Base Metal zone is unrelated to the PGE reef; (2) the Base Metal zone is an accumulation of the same sulfide found in the PGE reef, but this sulfide has only undergone fractionation in the Base Metal zone; or (3) the Base Metal zone is part of the same system as the PGE

Downloaded from http://pubs.geoscienceworld.org/segweb/economicgeology/article-pdf/120/4/997/7306637/5159_canham+et+al.pdf
by University of the Witwatersrand user

reef but represents an earlier (fractionated) high-tenor sulfide liquid.

Thompson et al. (2025c) do not distinguish the Base Metal zone and PGE reef in the Sandsloot deep Platreef (Fig. 1B) as distinct magmatic pulses, as they have similar geochemical signatures. However, this study shows that the sulfides and associated PGEs in the PGE reef and the Base Metal zone do not appear to be genetically related. Therefore, it is possible that the sequence may have been made up of chemically similar pulses of magma, but preserves two distinct generations of sulfide.

Conclusions

The Base Metal zone, located in the deep Platreef at Sandsloot, represents a new style of mineralization in the context of the Northern limb. It is distinct from other sulfide-enriched portions along the base of the Platreef, as it has very high (Os + Ir + Rh + Ru)/(Pt + Pd) ratios, being an IPGE + Rh-dominant zone opposed to Pt + Pd. The Base Metal zone is Fe sulfide rich and contains predominantly pyrrhotite-dominant magmatic sulfides, with lesser pentlandite and chalcopyrite. It has a PGM assemblage dominated by laurite and IPGE + Pt arsenosulfides, which are typically closely associated with sulfide. Pentlandite and pyrrhotite also host IPGEs + Rh, whereas Pd is almost exclusively hosted by pentlandite.

We propose the Base Metal zone represents the monosulfide solid solution portion of a sulfide liquid body, resulting in very high IPGE contents and high (IPGE + Rh)/(Pt + Pd) and Ni/Cu ratios. The sulfide liquid fractionated downward through the Base Metal zone, producing intermediately fractionated sulfides, with lower (Os + Ir + Rh + Ru)/(Pt + Pd) ratios toward the base of the Base Metal zone (Fig. 15B). The Cu + Pt + Pd + Au-poor nature of the Base Metal zone is the result of migration of Cu-rich sulfide liquids away from monosulfide solid solution during solidification of the melt (Fig. 15C). Dilution of tenors by addition of crustal S, or variable R-factor regimes, is responsible for the tenor variations between low-PGE tenor massive/semimassive sulfides and high-PGE tenor disseminated/blebby sulfides (Fig. 15D).

Further understanding of the fractionation trend throughout the Base Metal zone may benefit future exploration, as the Base Metal zone represents a monosulfide solid solution portion of the parental sulfide liquid, which fractionated downwards. This suggests a Cu-rich portion, with associated Pt + Pd + Au, may be present at greater depths, not yet intersected by drilling. Alternatively, the Cu-rich residual liquid was mobilized away from Sandsloot.

Acknowledgments

This research was funded by Anglo American through the Northern Limb in 4D (NL4D) consortium, awarded to the University of Leicester, Cardiff University, and University of Exeter. The Society of Economic Geologists (SEG) provided additional funding for geochemical and SEM analysis through the SEG Foundation Student Research Grant SRG 23-84. We also acknowledge Anglo American for logistical support with fieldwork and providing access to drill cores for sampling and downhole assay data. Additionally, we thank Lin Marvin for assistance with XRF analysis, Annika Burns for preparation of thin sections, Adam Cox for assistance with LA-ICP-MS analysis, and Leon Hicks for assistance with SEM analysis. We are grateful for the reviews of M.C. Jenkins and an anonymous reviewer and editorial handling by Dave Cooke, who helped to improve the quality and focus of the manuscript.

REFERENCES

Armitage, P.E.B., McDonald, I., Edwards, S.J., and Manby, G.M., 2002, Platinum-group element mineralization in the Platreef and calc-silicate footwall at Sandsloot, Potgietersrus District, South Africa: Applied Earth Science, v. 111, no. 1, p. 36–45.

Ashwal, L.D., Webb, S.J., and Knoper, M.W., 2005, Magmatic stratigraphy in the Bushveld Northern Lobe: Continuous geophysical and mineralogical data from the 2950 m Bellevue drillcore: South African Journal of Geology, v. 108, no. 2, p. 199–232.

Barnes, S.-J., and Lightfoot, P.C., 2005, Formation of magmatic nickel-sulfide ore deposits and processses affecting their copper and platinum-group element contents: Economic Geology, 100th Anniversary Volume, p. 179–213.

Barnes, S.-J., Makovicky, E., Makovicky, M., Rose-Hansen, J., and Karup-Moller, S., 1997, Partition coefficients for Ni, Cu, Pd, Pt, Rh, and Ir between monosulfide solid solution and sulfide liquid and the formation of compositionally zoned Ni-Cu sulfide bodies by fractional crystallization of sulfide liquid: Canadian Journal of Earth Sciences, v. 34, no. 4, p. 366–374.

Barnes, S.J., and Liu, W., 2012, Pt and Pd mobility in hydrothermal fluids: Evidence from komatiites and from thermodynamic modelling: Ore Geology Reviews, v. 44, p. 49–58.

Barnes, S.J., Taranovic, V., Schoneveld, L.E., et al., 2020, The occurrence and origin of pentlandite-chalcopyrite-pyrrhotite loop textures in magmatic Ni-Cu sulfide ores: Economic Geology, v. 115, no. 8, p. 1777–1798.

Blanks, D.E., Holwell, D.A., Barnes, S.J., et al., 2022, Mobilization and fractionation of magmatic sulfide: Emplacement and deformation of the Munali Ni-(Cu-platinum group element) deposit, Zambia: Economic Geology, v. 117, no. 8, p. 1709–1729.

Brownscombe, W., Ihlenfeld, C., Coppard, J., et al., 2015, The Sakatti Cu-Ni-PGE sulfide deposit in northern Finland, *in* Maier, W.D., Lahtinen, R., and O'Brien, H., eds., Mineral deposits of Finland: Elsevier, p. 211–252.

Buchanan, D.L., and Rouse, J.E., 1984, Role of contamination in the precipitation of sulphides in the Platreef of the Bushveld complex, *in* Buchanan, D.L., and Jones, J.M., eds., Sulfide deposits in mafic and ultramafic rocks: London, Institution of Mining and Metallurgy, p. 141–146.

Buchanan, D.L., Nolan, J., Suddaby, P., et al., 1981, The genesis of sulfide mineralization in a portion of the Potgietersrus limb of the Bushveld Complex: Economic Geology, v. 76, no. 3, p. 568–579.

Canham. K.R., Holwell. D.A., McDonald, I., et al.., 2025, Lower zone-hosted chromitite PGE-Ni-Cu mineralization at Zwartfontein, northern Bushveld Complex, South Africa: The role of chromite and volatiles: Economic Geology, v. 120, no. 2, p. 403–433, doi: 10.5382/econgeo.5145.

Cawthorn, R.G., 1999, Platinum-group element mineralization in the Bushveld Complex—a critical reassessment of geochemical models: South African Journal of Geology, v. 102, p. 268–281.

Chashchin, V.V., Petrov, S.V., Kiseleva, D.V., and Savchenko, Ye.E., 2021, Platinum content and formation conditions of the sulfide PGE-Cu-Ni Nyud-II deposit of the Monchegorsk pluton, Kola Peninsula, Russia: Geology of Ore Deposits, v. 63, no. 2, p. 87–117.

Chen, L.-M., Song, X.-Y., Keays, R.R., et al., 2013, Segregation and fractionation of magmatic Ni-Cu-PGE sulfides in the Western Jinchuan Intrusion, northwestern China: Insights from platinum group element geochemistry: Economic Geology, v. 108, no. 8, p. 1793–1811.

Cherdantseva, M., Vishnevskiy, A., Jugo, P.J., et al., 2023, Caught in the moment: Interaction of immiscible carbonate and sulfide liquids in mafic silicate magma—insights from the Rudniy intrusion (NW Mongolia): Mineralium Deposita, v. 59, p. 733–755.

Dare, S.A.S., Barnes, S.-J., Prichard, H.M., and Fisher, P.C., 2010a, The timing and formation of platinum-group minerals from the Creighton Ni-Cu-platinum group element sulfide deposit, Sudbury, Canada: Early crystallization of PGE-rich sulfarsenides: Economic Geology, v. 105, no. 6, p. 1071–1096.

Dare, S.A.S., Barnes, S.-J., and Prichard, H.M., 2010b, The distribution of platinum group elements (PGE) and other chalcophile elements among sulfides from the Creighton Ni-Cu-PGE sulfide deposit, Sudbury, Canada, and the origin of palladium in pentlandite: Mineralium Deposita, v. 45, no.

Downloaded from http://pubs.geoscienceworld.org/segweb/economicgeology/article-pdf/120/4/997/7306637/5159_canham+et+al.pdf
by University of the Witwatersrand user

8, p. 765–793.
Dare, S.A.S., Barnes, S.-J., Prichard, H.M., and Fisher, P.C., 2014, Mineralogy and geochemistry of Cu-rich ores from the McCreedy East Ni-Cu-PGE deposit (Sudbury, Canada): Implications for the behavior of platinum group and chalcophile elements at the end of crystallization of a sulfide liquid: Economic Geology, v. 109, no. 2, p. 343–366.
Ding, X., Ripley, E.M., and Li, C., 2012, PGE geochemistry of the Eagle Ni-Cu-(PGE) deposit, upper Michigan: Constraints on ore genesis in a dynamic magma conduit: Mineralium Deposita, v. 47, no. 1, p. 89–104.
Fischer-Gödde, M., Becker, H., and Wombacher, F., 2010, Rhodium, gold and other highly siderophile element abundances in chondritic meteorites: Geochimica et Cosmochimica Acta, v. 74, no. 1, p. 356–379.
Fleet, M.E., Chryssoulis, S.L., Stone, W.E., and Weisener, C.G., 1993, Partitioning of platinum-group elements and Au in the Fe-Ni-Cu-S system: Experiments on the fractional crystallization of sulfide melt: Contributions to Mineralogy and Petrology, v. 115, no. 1, p. 36–44.
Godel, B., Barnes, S.-J., and Maier, W.D., 2007, Platinum-group elements in sulphide minerals, platinum-group minerals, and whole-rocks of the Merensky reef (Bushveld Complex, South Africa): Implications for the rormation of the reef: Journal of Petrology, v. 48, no. 8, p. 1569–1604.
Grobler, D.F., Brits, J.A.N., Maier, W.D., and Crossingham, A., 2019, Litho- and chemostratigraphy of the Flatreef PGE deposit, northern Bushveld Complex: Mineralium Deposita, v. 54, no. 1, p. 3–28.
Hall, A., 1932, The Bushveld Igneous Complex in the central Transvaal: Geological Survey of South Africa, Memoir 28, 560 p.
Harris, C., and Chaumba, J.B., 2001, Crustal contamination and fluid-rock interaction during the formation of the Platreef, Northern limb of the Bushveld Complex, South Africa: Journal of Petrology, v. 42, no. 7, p. 1321–1347.
Helmy, H.M., and Bragagni, A., 2017, Platinum-group elements fractionation by selective complexing, the Os, Ir, Ru, Rh-arsenide-sulfide systems above 1020°C: Geochimica et Cosmochimica Acta, v. 216, p. 169–183.
Helmy, H.M., Ballhaus, C., Wohlgemuth-Ueberwasser, C., Fonseca, R.O.C., and Laurenz, V., 2010, Partitioning of Se, As, Sb, Te and Bi between monosulfide solid solution and sulfide melt—Application to magmatic sulfide deposits: Geochimica et Cosmochimica Acta, v. 74, no. 21, p. 6174–6179.
Helmy, H.M., Ballhaus, C., Fonseca, R.O.C., and Nagel, T.J., 2013, Fractionation of platinum, palladium, nickel, and copper in sulfide-arsenide systems at magmatic temperature: Contributions to Mineralogy and Petrology, v. 166, no. 6, p. 1725–1737.
Holwell, D.A., and McDonald, I., 2006, Petrology, geochemistry and the mechanisms determining the distribution of platinum-group element and base metal sulphide mineralisation in the Platreef at Overysel, northern Bushveld Complex, South Africa: Mineralium Deposita, v. 41, p. 575–598.
——2007, Distribution of platinum-group elements in the Platreef at Overysel, northern Bushveld Complex: A combined PGM and LA-ICP-MS study: Contributions to Mineralogy and Petrology, v. 154, no. 2, p. 171–190.
——2010, A review of the behaviour of platinum group elements within natural magmatic sulfide ore systems: Platinum Metals Review, v. 54, p. 26–36.
Holwell, D.A., McDonald, I., and Armitage, P.E.B., 2006, Platinum-group mineral assemblages in the Platreef at the Sandsloot mine, northern Bushveld Complex, South Africa: Mineralogical Magazine, v. 70, no. 1, p. 83–101.
Holwell, D.A., Boyce, A.J., and McDonald, I., 2007, Sulfur isotope variations within the Platreef Ni-Cu-PGE deposit: Genetic implications for the origin of sulfide mineralization: Economic Geology, v. 102, no. 6, p. 1091–1110.
Holwell, D.A., McDonald, I., and Butler, I.B., 2011, Precious metal enrichment in the Platreef, Bushveld Complex, South Africa: Evidence from homogenized magmatic sulfide melt inclusions: Contributions to Mineralogy and Petrology, v. 161, no. 6, p. 1011–1026.
Holwell, D.A., Keays, R.R., McDonald, I., and Williams, M.R., 2015, Extreme enrichment of Se, Te, PGE and Au in Cu sulfide microdroplets: Evidence from LA-ICP-MS analysis of sulfides in the Skaergaard Intrusion, east Greenland: Contributions to Mineralogy and Petrology, v. 170, no. 53, doi: 10.1007/s00410-015-1203-y.
Holwell, D.A., Adeyemi, Z., Ward, L.A., et al., 2017, Low temperature alteration of magmatic Ni-Cu-PGE sulfides as a source for hydrothermal Ni and PGE ores: A quantitative approach using automated mineralogy: Ore Geology Reviews, v. 91, p. 718–740.
Hutchinson, D., and Kinnaird, J.A., 2005, Complex multistage genesis for the Ni-Cu-PGE mineralisation in the southern region of the Platreef, Bushveld Complex, South Africa: Applied Earth Science, v. 114, p. 208–224.
Ihlenfeld, C., and Keays, R.R., 2011, Crustal contamination and PGE mineralization in the Platreef, Bushveld Complex, South Africa: Evidence for multiple contamination events and transport of magmatic sulfides: Mineralium Deposita, v. 46, no. 7, p. 813–832.
Jones, R.E., 2013, Petrological and geochemical study of Platreef chromitites, northern Bushveld, South Africa: Ph.D. thesis, Cardiff, Cardiff University, 280 p.
Kawohl, A., Whymark, W.E., Bite, A., and Frimmel, H.E., 2020, High-grade magmatic platinum group element-Cu(-Ni) sulfide mineralization associated with the Rathbun offset dike of the Sudbury Igneous Complex (Ontario, Canada): Economic Geology, v. 115, no. 3, p. 505–525.
Kelly, D.P., and Vaughan, D.J., 1983, Pyrrhotine-pentlandite ore textures: a mechanistic approach: Mineralogical Magazine, v. 47, p. 453–463.
Kinnaird, J.A., and McDonald, I., 2018, The Northern limb of the Bushveld Complex: A new economic frontier: Society of Economic Geologists, Special Publication 21, p. 157–176.
Kinnaird, J.A., Hutchinson, D., Schurmann, L., Nex, P.A.M., and de Lange, R., 2005, Petrology and mineralisation of the southern Platreef: Northern limb of the Bushveld Complex, South Africa: Mineralium Deposita, v. 40, p. 576–597.
Kitakaze, A., and Sugaki, A., 2004, The phase relations between $Fe_{4.5}Ni_{4.5}S_8$ and Co_9S_8 in the system Fe-Ni-Co-S at temperatures from 400° to 1100°C: Canadian Mineralogist, v. 42, p. 17–42.
Kitakaze, A., Machida, T., and Komatsu, R., 2016, Phase relations in the Fe-Ni-S system from 875 to 650°C: The Canadian Mineralogist, v. 54, no. 5, p. 1175–1186.
Li, C., Barnes, S.-J., Makovicky, E., Rose-Hansen, J., and Makovicky, M., 1996, Partitioning of nickel, copper, iridium, rhenium, platinum, and palladium between monosulfide solid solution and sulfide liquid: Effects of composition and temperature: Geochimica et Cosmochimica Acta, v. 60, no. 7, p. 1231–1238.
Liang, Q.-L., Song, X.-Y., Wirth, R., Chen, L.-M., and Dai, Z.-H., 2019, Implications of nano- and micrometer-size platinum-group element minerals in base metal sulfides of the Yangliuping Ni-Cu-PGE sulfide deposit, SW China: Chemical Geology, v. 517, p. 7–21.
Liu, W., Migdisov, A., and Williams-Jones, A., 2012, The stability of aqueous nickel(II) chloride complexes in hydrothermal solutions: Results of UV-visible spectroscopic experiments: Geochimica et Cosmochimica Acta, v. 94, p. 276–290.
Liu, Y., and Brenan, J., 2015, Partitioning of platinum-group elements (PGE) and chalcogens (Se, Te, As, Sb, Bi) between monosulfide-solid solution (MSS), intermediate solid solution (ISS) and sulfide liquid at controlled f_{O_2}-f_{S_2} conditions: Geochimica et Cosmochimica Acta, v. 159, p. 139–161.
Maier, W.D., de Klerk, L., Blaine, J., et al., 2008, Petrogenesis of contact-style PGE mineralization in the northern lobe of the Bushveld Complex: Comparison of data from the farms Rooipoort, Townlands, Drenthe and Nonnenwerth: Mineralium Deposita, v. 43, no. 3, p. 255–280.
Maier, W.D., Abernethy, K.E.L., Grobler, D.F., and Moorhead, G., 2021, Formation of the Flatreef deposit, northern Bushveld, by hydrodynamic and hydromagmatic processes: Mineralium Deposita, v. 56, p. 11–30.
Maier, W.D., Barnes, S.J., Godel, B.M., Grobler, D., and Smith, W.D., 2023, Petrogenesis of thick, high-grade PGE mineralisation in the Flatreef, northern Bushveld Complex: Minerlium Deposita, v. 58, p. 881–902, doi: 10.1007/s00126-022-01156-6.
Mansur, E.T., Barnes, S.-J., and Duran, C.J., 2019, Textural and compositional evidence for the formation of pentlandite via peritectic reaction: Implications for the distribution of highly siderophile elements: Geology, v. 47, no. 4, p. 351–354.
Mansur, E.T., Barnes, S.-J., Duran, C.J., and Sluzhenikin, S.F., 2020, Distribution of chalcophile and platinum-group elements among pyrrhotite, pentlandite, chalcopyrite and cubanite from the Noril'sk-Talnakh ores: Implications for the formation of platinum-group minerals: Mineralium Deposita, v. 55, no. 6, p. 1215–1232.
Mansur, E.T., Barnes, S.-J., and Duran, C.J., 2021, An overview of chalcophile element contents of pyrrhotite, pentlandite, chalcopyrite, and pyrite from magmatic Ni-Cu-PGE sulfide deposits: Mineralium Deposita, v. 56, p. 179–204.
Martin, T., 2018, Characterisation and spatial analysis of the platinum-group mineralogy on Tweefontein Hill & Turfspruit properties, northern Bushveld Complex, South Africa: MSc thesis, Camborne, University of Exeter, 95 p.
McDonald, I., and Holwell, D.A., 2007, Did lower zone magma conduits store PGE-rich sulphides that were later supplied to the Platreef?: South African Journal of Geology, v. 110, no. 4, p. 611–616.
——2011, Geology of the Northern Bushveld Complex and the setting and

Downloaded from http://pubs.geoscienceworld.org/segweb/economicgeology/article-pdf/120/4/997/7306637/5159_canham+et+al.pdf
by University of the Witwatersrand user

genesis of the Platreef Ni-Cu-PGE deposit: Reviews in Economic Geology, v. 17, p. 297–327.
McDonald, I., Holwell, D.A., and Armitage, P.E.B., 2005, Geochemistry and mineralogy of the Platreef and "'Critical zone"' of the northern lobe of the Bushveld Complex, South Africa: Implications for Bushveld stratigraphy and the development of PGE mineralisation: Mineralium Deposita, v. 40, p. 526–549.
McDonald, I., Holwell, D.A., and Wesley, B., 2009, Assessing the potential involvement of an early magma staging chamber in the generation of the Platreef Ni-Cu-PGE deposit in the northern limb of the Bushveld Complex: A pilot study of the Lower Zone Complex at Zwartfontein: Applied Earth Science, v. 118, no. 1, p. 5–20.
McFall, K., McDonald, I., Tanner, D., and Harmer, R.E., 2019, The mineralogy and mineral associations of platinum-group elements and precious metals in the Aurora Cu-Ni-Au-PGE deposit, northern limb, Bushveld Complex: Ore Geology Reviews, v. 106, p. 403–422, doi: 10.1016/j.oregeorev.2019.02.008.
Mudd, G.M., Jowitt, S.M., and Werner, T.T., 2018, Global platinum group element resources, reserves and mining—A critical assessment: Science of The Total Environment, v. 622–623, p. 614–625.
Mungall, J.E., Andrews, D.R.A., Cabri, L.J., Sylvester, P.J., and Tubrett, M., 2005, Partitioning of Cu, Ni, Au, and platinum-group elements between monosulfide solid solution and sulfide melt under controlled oxygen and sulfur fugacities: Geochimica et Cosmochimica Acta, v. 69, no. 17, p. 4349–4360.
Naldrett, A.J., Asif, M., Scandl, E., et al., 1999, Platinum-group elements in the Sudbury ores; significance with respect to the origin of different ore zones and to the exploration for footwall orebodies: Economic Geology, v. 94, no. 2, p. 185–210.
Naldrett, A.J., Asif, M., Krstic, S., and Li, C., 2000, The composition of mineralization at the Voisey's Bay Ni-Cu sulfide deposit, with special reference to platinum-group elements: Economic Geology, v. 95, no. 4, p. 845–865.
Naldrett, A.J., Kinnaird, J., Wilson, A., et al., 2009, Chromite composition and PGE content of Bushveld chromitites: Part 1 – the Lower and Middle Groups: Applied Earth Science, v. 118, nos. 3–4, p. 131–161.
Nex, P.A.M., 2005, The structural setting of mineralisation on Tweefontein Hill, northern limb of the Bushveld Complex, South Africa: Applied Earth Science, v. 114, p. 243–251.
Osbahr, I., Klemd, R., Oberthür, T., Brätz, H., and Schouwstra, R., 2013, Platinum-group element distribution in base-metal sulfides of the Merensky Reef from the eastern and western Bushveld Complex, South Africa: Mineralium Deposita, v. 48, no. 2, p. 211–232.
Palme, H., and O'Neill, H.St.C., 2014, 3.1 - cosmochemical estimates of mantle composition, *in* Holland, H.D., and Turekian, K.K., eds., Treatise on geochemistry, 2nd ed.: Oxford, Elsevier, p. 1–39.
Piercey, S., 2014, Modern analytical facilities 2: A review of quality assurance and quality control (QA/QC) procedures for lithogeochemical data: Journal of the Geological Association of Canada/Geoscience Canada, v. 41, no. 1, p. 75–88.
Piña, R., Gervilla, F., Helmy, H., Fonseca, R.O.C., and Ballhaus, C., 2020, Partition behavior of platinum-group elements during the segregation of arsenide melts from sulfide magma: American Mineralogist, v. 105, no. 12, p. 1889–1897.
Queffurus, M., and Barnes, S.-J., 2015, A review of sulfur to selenium ratios in magmatic nickel-copper and platinum-group element deposits: Ore Geology Reviews, v. 69, p. 301–324.
Scoon, R.N., and Teigler, B., 1994, Platinum-group element mineralization in the critical zone of the western Bushveld Complex; I, Sulfide poor-chromitites below the UG-2: Economic Geology, v. 89, no. 5, p. 1094–1121.
Sharman-Harris, E.R., Kinnaird, J.A., Harris, C., and Horstmann, U.E., 2005, A new look at sulphide mineralisation of the Northern limb, Bushveld Complex: A stable isotope study: Applied Earth Science, v. 114, no. 4, p. 252–263.
Smith, J.W., Holwell, D.A., and McDonald, I., 2014, Precious and base metal geochemistry and mineralogy of the Grasvally Norite-Pyroxenite-Anorthosite (GNPA) member, northern Bushveld Complex, South Africa: Implications for a multistage emplacement: Mineralium Deposita, v. 49, no. 6, p. 667–692.
Smith, J.W., Holwell, D.A., McDonald, I., and Boyce, A.J., 2016, The application of S isotopes and S/Se ratios in determining ore-forming processes of magmatic Ni-Cu-PGE sulfide deposits: A cautionary case study from the northern Bushveld Complex: Ore Geology Reviews, v. 73, p. 148–174.
Sullivan, N.A., Zajacz, Z., Brenan, J.M., and Tsay, A., 2022, The solubility of platinum in magmatic brines: Insights into the mobility of PGE in ore-forming environments: Geochimica et Cosmochimica Acta, v. 316, p. 253–272.
Thériault, R.D., Barnes, S.-J., and Severson, M.J., 1997, The influence of country-rock assimilation and silicate to sulfide ratios (R factor) on the genesis of the Dunka Road Cu-Ni-platinum-group element deposit, Duluth Complex, Minnesota: Canadian Journal of Earth Sciences, v. 34, no. 4, p. 375–389.
Thompson, E.S., Holwell, D.A., McDonald, I., et al., 2025a, The effects of carbonate contamination on Ni-Cu-PGE deposit genesis in the Platreef, northern Bushveld Complex: A case study using Niggli Numbers: Chemical Geology, v. 671, no. 5, article 122481, doi: 10.1016/j.chemgeo.2024.122481.
Thompson, E.S., Holwell, D.A., McDonald, I., et al., 2025b, Magmatic stratigraphy and platinum group element mineralization at Tweefontein, northern Bushveld Complex: Evidence of a complex intrusion history of Lower, Critical and Main zone magmas: Economic Geology, v. 120, p. 1–27, doi: 10.5382/econgeo.5123.
Thompson, E.S., Holwell, D.A., McDonald, I., et al., 2025c, Magmatic stratigraphy of the deep Platreef at Sandsloot, northern Bushveld Complex: Carbonate contamination and controls on Ni-Cu-PGE mineralization: Economic Geology, v. 120, p. 973–996.
Tolstykh, N., Brovchenko, V., Rad'ko, V., et al., 2022, Rh, Ir, and Ru partitioning in the Cu-poor IPGE massive ores, Talnakh Intrusion, Skalisty mine, Russia: Minerals, v. 12, no. 1, p. 18.
van der Merwe, F., Viljoen, F., and Knoper, M., 2012, The mineralogy and mineral associations of platinum group elements and gold in the Platreef at Zwartfontein, Akanani Project, northern Bushveld Complex, South Africa: Mineralogy and Petrology, v. 106, nos. 1–2, p. 25–38.
van der Merwe, M.J., 1976, The layered sequence of the Potgietersrus limb of the Bushveld Complex: Economic Geology, v. 71, no. 7, p. 1337–1351.
——2008, The geology and structure of the Rustenburg Layered Suite in the Potgietersrus/Mokopane area of the Bushveld Complex, South Africa: Mineralium Deposita, v. 43, no. 4, p. 405–419.
White, J.A., 1994, The Potgietersrus prospect—geology and exploration history: South African Institute of Mining and Metallurgy Symposium Series, v. 3, p. 173–181.
Yudovskaya, M., Kinnaird, J., Naldrett, A.J., et al., 2011, Facies variation in PGE mineralization in the central Platreef of the Bushveld Complex, South Africa: The Canadian Mineralogist, v. 49, no. 6, p. 1349–1384.
Yudovskaya, M.A., Kinnaird, J.A., Grobler, D.F., et al., 2017, Zonation of Merensky-style platinum-group element mineralization in Turfspruit thick reef facies (Northern limb of the Bushveld Complex): Economic Geology, v. 112, no. 6, p. 1333–1365.
Zeh, A., Ovtcharova, M., Wilson, A.H., and Schaltegger, U., 2015, The Bushveld Complex was emplaced and cooled in less than one million years—results of zirconology, and geotectonic implications: Earth and Planetary Science Letters, v. 418, p. 103–114.



Kate Canham is a contract geologist with Gnomic Exploration Services, based in Queensland, Australia. She received her MSc from the University of Leicester in 2020, where she investigated supergene Cu-Au mineralization at the Kitumba iron oxide copper-gold (IOCG) deposit in Zambia. She completed her PhD in early 2025, focusing on the postemplacement controls on platinum group element (PGE)-Ni-Cu mineralization in the northern Bushveld Complex, South Africa. Her research integrates mineralogy, whole-rock and mineral chemistry, and S isotopes to assess the roles of magmatic, contamination, and hydrothermal processes.

Downloaded from http://pubs.geoscienceworld.org/segweb/economicgeology/article-pdf/120/4/997/7306637/5159_canham+et+al.pdf
by University of the Witwatersrand user

Downloaded from http://pubs.geoscienceworld.org/segweb/economicgeology/article-pdf/120/4/997/7306637/5159_canham+et+al.pdf
by University of the Witwatersrand user